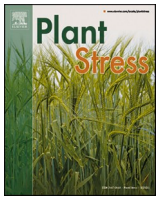
Plant Stress 21 (2026) 101397



Contents lists available at ScienceDirect

Plant Stress

journal homepage: www.sciencedirect.com/journal/plant-stress





Deciphering the molecular mechanisms of maize defence against the fall armyworm (*Spodoptera frugiperda*) through integrated transcriptomics and metabolomics

Patne Nagesh [a], Onkarappa Dhanyakumar [b], Jagdish Jaba [b], Kalenahalli Yogendra [b,*], Jayasaravanan Desika [a,c], Nivedita Shettigar [a,d,e], Revanayya M. Gothe [b], Sagala Murali Mohan [a], Pulime Bhaskara Naidu [a], Suraj Prashad Mishra [b], Sudha K. Nair [a], Bindiganavile Sampath Vivek [a,*]

[a] *International Maize and Wheat Improvement Center (CIMMYT), Hyderabad, India*
[b] *International Crops Research Institute for the Semi-Arid Tropics (ICRISAT), Hyderabad, India*
[c] *V.O.C. Agricultural College and Research Institute, Tamil Nadu Agricultural University (TNAU), Killikulam 628252, India*
[d] *Department of Genetics and Plant Breeding, Professor Jayashankar Telangana Agricultural University, Hyderabad, India*
[e] *ICAR-Regional Complex North Eastern Hill, Umiam, Meghalaya 793103, India*

ARTICLE INFO

Keywords:
Fall armyworm
Host-plant resistance
Maize
Metabolomics
Transcriptomics

ABSTRACT

The fall armyworm (FAW), *Spodoptera frugiperda*, is a highly destructive polyphagous pest that threatens maize production worldwide, particularly in tropical and subtropical agroecosystems. Understanding the molecular basis of host plant resistance is critical for developing durable and sustainable pest management strategies. In this study, we used an integrated transcriptomic and metabolomic approach to dissect defense responses in contrasting maize inbred lines, the resistant CML338 and the susceptible CML451, under FAW-infested and uninfested conditions. RNA-seq generated high-quality datasets with mapping efficiencies of 84–87 % and revealed extensive transcriptional reprogramming in the resistant genotype following infestation. Multivariate analyses showed clear genotype- and treatment-dependent separation, with principal components explaining >60 % of the total variance. Differentially expressed genes were significantly enriched in pathways related to phytohormone signaling, MAPK cascades, transcriptional regulation, fatty acid metabolism, and secondary metabolite biosynthesis. Untargeted LC—HRMS metabolomics revealed pronounced accumulation of putative resistance-related metabolites in CML338, including fatty acids (linoleic acid, and arachidonic acid) and terpenoids (α-terpineol, capsorubin, 5-hydroxyzeaxanthin, meso-zeaxanthin, and violaxanthin). Integrated transcriptome–metabolome correlation analysis (PCC $\geq$ 0.85, $P \leq 0.05$) demonstrated tight coordination between metabolite accumulation and the expression of key biosynthetic genes, including *TPS, DXS, PLD, LOX*, and *FAD*. Furthermore, *in-silico* molecular docking showed strong binding of α-terpineol to the FAW gut enzyme Aminopeptidase N1 (−6.6 kcal mol^{-1}), suggesting a potential interaction; however, this is a putative prediction based on computational analysis and requires biochemical and bioassay validation for confirmation. Collectively, this study provides a systems-level understanding of maize–FAW interactions and identifies candidate genes, pathways, and metabolites for breeding insect-resistant maize cultivars.

1. Introduction

Fall armyworm (FAW), *Spodoptera frugiperda* (Lepidoptera: Noctuidae), is a highly polyphagous and generalist insect species that can feed on over 100 plant species, including economically important crops such as maize, sorghum, rice, and cotton. However, maize remains its most preferred host due to its nutritional content and wide availability across growing regions (Goergen et al., 2016). FAW has demonstrated a remarkable ability to migrate over long distances and establish itself in diverse agro-ecological zones. Its spread has been facilitated by a

* Corresponding authors.
E-mail addresses: Yogendra.Kalenahalli@icrisat.org (K. Yogendra), bindivivek@gmail.com (B.S. Vivek).

https://doi.org/10.1016/j.stress.2026.101397
Received 17 January 2026; Received in revised form 6 April 2026; Accepted 24 April 2026
Available online 28 April 2026
2667-064X/© 2026 The Author(s). Published by Elsevier B.V. This is an open access article under the CC BY license (http://creativecommons.org/licenses/by/4.0/).

combination of its strong flying ability, high reproductive potential, and adaptability to different climates (Nagoshi et al., 2018). FAW is originally native to the tropical and subtropical regions of the Americas. Due to its migratory ability, it has moved across all parts of the world (Goergen et al., 2016; Prasanna et al., 2018). FAW infestations cause severe damage to maize by feeding on foliage, whorls, and ears, leading to stunted growth and reduced yields. Losses can range from 20 % to 50 %, posing a serious threat to food security and farmer livelihoods in low- and middle-income countries (Deshmukh et al., 2021; Hruska, 2019; Nagoshi et al., 2019; Prasanna et al., 2018). In response to rising FAW infestations, smallholder maize farmers in Asia and Africa have shifted towards greater pesticide use, with limited reliance on cultural control (Hruska, 2019). Commonly used insecticides like organophosphates and pyrethroids are broad-spectrum and have been linked to evolutionary pressure on FAW to develop resistance to these insecticides (Day et al., 2017), while also harming potential natural enemies (Harrison et al., 2019; Onkarappa et al., 2023).

Due to a primary focus on breeding for higher yields, many commercial maize cultivars have lost key defense-related traits crucial for resistance against FAW. As a result, host plant resistance (HPR) has emerged as a promising and sustainable approach for managing FAW infestations and is increasingly being adopted globally (Chiriboga Morales et al., 2021; de Paiva et al., 2016). Many research groups have developed phenotyping methods to evaluate leaf damage at different plant growth stages, identifying the differential response of maize genotypes to FAW. This enables the development of breeding strategies that can pyramid the various genes involved. These assessments usually involve infesting young seedlings with neonate larvae to detect resistance from the early stages of plant development (Ni et al., 2014; Soujanya et al., 2022) and beyond until cob development. To date, few commercial maize varieties in Asia and Africa have been reported to possess resistance to FAW, and breeding efforts for FAW resistance remain limited in the region (Kasoma et al., 2021; Matova et al., 2020). In contrast, several maize landraces and germplasm with natural resistance to FAW have been identified in the Americas, Asia, and Africa (Prasanna et al., 2022). This disparity is partially due to trade-offs of modern breeding programs, where selection for higher yield has led to the loss of certain defensive traits in maize (Bellota et al., 2013; De Lange et al., 2014).

In plants, defense strategies to counter insect herbivory are complex and are generally categorized into direct and indirect resistance mechanisms (Mithöfer et al., 2012). Upon herbivore attack, the bioactive form of Jasmonic Acid (JA) is known to trigger a cascade of defense responses that include the production of protective secondary metabolites (Erb et al., 2019). These compounds can be present constitutively or synthesized in response to damage, acting as toxins or deterrents that disrupt insect development and feeding behaviour (Howe et al., 2008). Rapid production of these diverse metabolites indicates a plant's adaptive capacity to defend itself under herbivore pressure. Moreover, recent advancements in the integration of omics technologies have provided valuable insights into the mechanisms underlying resistance to insect herbivory (Gothe et al., 2024).

In maize, the integration of multi-omics approaches has become a powerful strategy for addressing FAW infestation by linking metabolic reprogramming with gene regulatory networks involved in plant defense (Desika et al., 2024). In the present study, we investigated the molecular basis of resistance in CIMMYT-developed maize inbred lines using integrated transcriptomic and untargeted metabolomic analyses. The 48 h post-infestation time point was strategically selected to capture early defense responses, characterized by active transcriptional and metabolic reconfiguration prior to extensive tissue damage. Here, resistance was defined phenotypically as lower leaf damage ratings in the resistant line compared to the susceptible line. By quantifying dynamic molecular changes in contrasting genotypes, we aimed to identify key defense genes and associated metabolites and to explore their potential functional relevance through in silico docking analyses, thereby providing a comprehensive systems-level understanding of maize–FAW interactions.

2. Materials and methods

2.1. Plant materials

Based on detailed evaluations of selected lines under greenhouse and laboratory conditions, including leaf bioassays conducted as no-choice artificial infestation (as per protocols of Sharma et al., 1997; Vashisth et al., 2024) with leaf damage scored on 1–9 scale (Davis and Williams, 1992), CIMMYT maize lines, CML451 (susceptible parent, unpublished data) and CML338 (resistant parent) (Matova et al., 2022), were used for studying the metabolic responses to FAW infestation (Fig. S1). Ten seeds of each entry, in two sets, were sown during the wet season of 2023 in a net house under natural environmental conditions, with uniform irrigation and recommended fertilization to ensure healthy growth. Finally, three plants per pot were retained in each of three replications. Each seedling in each replicate was infested with two neonates which were two days old using a camel brush to place the larvae at the base of whorls (Vashisth et al., 2024). Treatment 1 involved infesting both the parents with FAW neonates twenty days after sowing, while Treatment 2 involved allowing both genotypes to grow as uninfested controls. Infested and non-infested treatments were both covered with a small net for 48 h to ensure that the infestation was contained to Treatment 1. Thus, the experiment consisted of four experimental groups: pest-infested resistant parent (CML338) (RP), non-infested resistant parent / control (resistant mock - RM), pest-infested susceptible parent (CML451) (SP), and non-infested susceptible parent / control (susceptible mock - SM). Each treatment had three biological replicates for transcriptomics (n = 12 RNA-seq samples) and five replicates for metabolomics (n = 20 metabolomics samples). Leaf tissue from both infested and non-infested control plots was carefully collected 48 h after infestation by avoiding contamination and handling stress. For each replicate, a composite leaf sample was obtained by pooling tissue from multiple seedlings within the same treatment to minimize biological variability. The samples were immediately flash-frozen in liquid nitrogen to halt metabolic activity and preserve the biochemical state at the time of collection. The frozen samples were stored at –80 °C until further processing for RNA-seq and metabolite extraction.

2.2. RNA-seq and functional annotation

Leaf tissues from FAW-infested and uninfested resistant and susceptible maize genotypes were used for transcriptome profiling. Total RNA was extracted using a Qiagen RNA isolation kit, and quality and quantity were assessed prior to sequencing on the Illumina NovaSeq 6000 platform at Bionivid Technology Pvt. Ltd. (Bengaluru, India). Raw FASTQ reads were processed using Fastp (v0.23.2) for adapter trimming and quality filtering (Phred score <30), and clean reads were aligned to the *Zea mays* reference genome (NCBI accession GCA_902167145.1; accessed 11 December 2024; https://www.ncbi.nlm.nih.gov/datasets/genome/GCF_902167145.1/) using HISAT2. Reference-guided transcript assembly and gene-level quantification were performed with StringTie (v2.1.4), and raw count matrices were generated using the prepDE.py script for differential expression analysis in DESeq2. FPKM and TPM values were calculated separately and used only for descriptive visualization and expression profiling, not for differential expression testing. Differentially expressed genes were identified using predefined statistical thresholds and categorized as resistance-related constitutive (RRC = RM > SM) or resistance-related induced [RRI= (RP/RM)>(SP/SM)] according to the specified contrasts.

2.2.1. Transcritomics data analysis

Transcriptome data were analyzed using RStudio (R version 4.4.2). Raw RNA-seq count data were imported into R and processed using the packages DESeq2, edgeR, and limma for quality filtering, normalization,

and differential expression analysis. Lowly expressed genes were filtered out prior to normalization, and library size correction was performed using the median-of-ratios method implemented in DESeq2 to account for sequencing depth and compositional bias. Variance stabilizing transformation (VST) or regularized log (rlog) transformation was applied to normalized counts to stabilize variance for downstream multivariate analyses. Principal Component Analysis (PCA) was conducted using the prcomp function and visualized with ggplot2 and FactoMineR to evaluate sample clustering and variability. Differentially expressed genes (DEGs) were identified based on adjusted *p*-values (Benjamini–Hochberg FDR ≤ 0.05) and $|\log_2 \text{fold change}| > 1.0$. Z-score normalization of gene expression values was performed using the R studio. Volcano plots were generated using Enhanced Volcano and ggplot2, heatmaps were constructed using pheatmap and Complex Heatmap, and Venn diagrams were produced using the VennDiagram package. Functional enrichment and pathway analyses were performed using the DAVID Bioinformatics Resources platform (https://davidbioinformatics.nih.gov/home.jsp), and Gene Ontology (GO) visualization was generated using SRplot (https://www.bioinformatics.com.cn/en), with significance determined at FDR ≤ 0.05.

2.3. Metabolite extraction and liquid chromatography-high-resolution mass spectroscopy (LC—HRMS) analysis

Treatment samples (100 mg) were ground in liquid nitrogen and extracted with 800 µL of ice-cold 80 % methanol containing 0.1 % formic acid. The mixture was vortexed for 1 min, incubated on an orbital shaker (100 rpm) for 15 min, and sonicated for 15 min at 40 kHz. After centrifugation (12,000 rpm, 10 min, 4 °C), the supernatant was collected and dried using a SpeedVac concentrator (Eppendorf). The residue was reconstituted in 200 µL of 80 % methanol with 0.1 % formic acid and filtered through a 0.22 µm hydrophilic PVDF filter (Millipore Millex-GV). A 50 µL aliquot was transferred to an autosampler vial and maintained at 10 °C. Untargeted metabolomic analysis was performed using UHPLC-Q-TOF-MS/MS (Xevo G2-XS, Waters, USA) (De Vos et al., 2007) operated exclusively in positive electrospray ionization (ESI^+) mode. Instrument parameters included a capillary voltage of 2.0 kV, cone voltage of 40 V, desolvation temperature of 400 °C, source temperature of 110 °C, desolvation gas flow of 800 L/h, cone gas flow of 50 L/h, scan time of 1 s, and a mass range of 50–2000 Da. Chromatographic separation was achieved on an Acquity UPLC BEH—C18 column (100 × 2.1 mm, 1.7 µm) at 30 °C using a gradient elution program. Data were acquired in centroid mode using multiplexed MS/MS (MSE) acquisition and recorded with MassLynx v4.1 software (Waters).

Quality control (QC) during LC–HRMS analysis included the use of leucine enkephalin as a lock-mass reference to correct mass drift and sodium iodide for system calibration prior to analysis. Blank injections were performed to monitor contamination and carryover, and samples were analyzed in randomized order to minimize systematic bias. Instrument stability and signal drift were evaluated through periodic QC injections and clustering patterns in multivariate analyses.

2.3.1. LC—HRMS output processing

LC—HRMS raw files (Waters format) were converted to mzXML format and processed in MZmine-2 using the high-sensitivity ADAP wavelet algorithm (Avuthu et al., 2024). Detected masses and intensities were exported, and inconsistent peaks, isotopes, and adducts were removed prior to downstream analysis.

2.3.2. Identification of resistance-related (RR) metabolites

Peak intensities of monoisotopic ions detected in positive ionization mode (primarily $[M + H]^+$ adducts) were statistically evaluated using pairwise Student's *t*-tests, and features significant at $p < 0.05$ (FDR $\leq$ 0.05) were retained. Metabolites showing significantly higher abundance in FAW-infested maize were classified as FAW-induced. For resistance-related (RR) metabolites, fold change in abundance was calculated relative to FAW-fed resistant genotypes. Putative metabolite identification was based on (1) accurate mass matching (AME < 10 ppm) against KEGG, LIPIDMAPS, and METLIN databases, and (2) fragmentation pattern match with those in databases or in silico verification. Metabolites more abundant in resistant than susceptible genotypes were defined as RR metabolites and further categorized as RR constitutive (RRC =RM > SM) or RR induced [RRI= (RP/RM)>(SP/SM)].

2.3.3. Metabolomic data analysis

Statistical analyses were performed using R Studio (version 4.4.2). Raw metabolite intensities were first median-normalized to correct for systematic variation across samples, followed by $\log_2$ transformation to stabilize variance and approximate normality. Subsequently, autoscaling (mean centering and standardization) was applied prior to multivariate analyses (PCA, PLS-DA). Metabolomic Pathway Analysis (MetPA) in MetaboAnalyst was employed to interpret metabolic changes, with pathways visualized as circles sized by impact score and colored according to *p*-values. Differentially accumulated metabolites were identified using $p < 0.05$ (FDR ≤ 0.05) and $|\log_2 FC| > 1.0$. Volcano plots were generated using SRplot (https://www.bioinformatics.com.cn/en?keywords=volcano), and Venn diagrams and heatmaps were created using the Venn Diagram tool (https://bioinformatics.psb.ugent.be/webtools/Venn/) and MeV software (v4.8, USA), respectively.

2.4. Weighted gene co-expression network analysis (WGCNA) of transcriptomes and metabolomes

WGCNA was conducted in R to identify co-expression modules associated with maize-fall armyworm (FAW) interactions by integrating transcriptomic and metabolomic datasets. The final datasets used for network construction consisted of 12 transcriptomic samples and 20 metabolomic samples. For transcriptomic analysis, lowly expressed genes were removed and count data were variance-stabilized using the DESeq2 package, after which the 10,000 most variable genes were retained to improve robustness of network construction and reduce noise given the moderate sample size. For metabolomics, raw metabolite intensities were $\log_2$-transformed, low-abundance features were filtered out, and the remaining metabolites were z-score normalized prior to analysis. Co-expression networks were constructed using the WGCNA package, where pairwise correlations were transformed into adjacency matrices using a soft-thresholding power selected based on the scale-free topology criterion, and subsequently converted into topological overlap matrices (TOM) to measure network interconnectedness. Modules of co-expressed genes or metabolites were identified using hierarchical clustering with dynamic tree cutting, followed by module merging at a cut height of 0.25, and module eigengenes were correlated with resistance and susceptibility traits. To control for multiple testing across module-trait associations, False Discovery Rate (FDR) correction was applied and associations were considered significant at FDR < 0.05. To further assess statistical robustness, 10,000 phenotype-label permutations were performed to generate empirical null distributions for module-trait correlations, and empirical permutation *p*-values were calculated as the proportion of permuted correlations exceeding the observed absolute correlation. In addition, stability of module-trait relationships was evaluated using leave-one-out resampling, in which each sample was sequentially removed and correlations recalculated to assess the consistency of module-trait associations. Key genes and metabolites from significant modules were subsequently visualized as association networks using the *igraph* and *ggraph* packages.

2.5. Correlation analysis of transcriptome and metabolome data

Pearson's correlation coefficients (PCCs) were calculated between differentially expressed genes (DEGs) and differentially accumulated metabolites (DAMs), as well as between genes and metabolites within the same pathways, using the *cor* package in R. Gene–metabolite pairs

with PCC $\geq$ 0.85 and $p \leq 0.05$ (FDR $\leq$ 0.05) were selected to generate heatmaps, nine-quadrant plots, and correlation networks, enabling the identification of DEGs and DAMs co-enriched in shared pathways.

2.6. Homology-based 3D modeling and molecular docking of aminopeptidase N (APN) and alkaline-phosphatase (ALP) in FAW

2.6.1. Retrieval of APN and ALP sequences and homology-based 3D modeling

Based on earlier reports (Mishra et al., 2019; Gómez et al., 2018; Flores-Escobar et al., 2013; Lee et al., 2014), two FAW midgut brush-border enzymes—aminopeptidase N (APN) and alkaline phosphatase (ALP)—were selected as targets for in silico interaction studies. Protein sequences of APN and ALP were obtained in FASTA format from the NCBI protein database (https://www.ncbi.nlm.nih.gov/protein), and only intact catalytic domains were retained for analysis. Three-dimensional structures were generated by homology modeling using SWISS-MODEL (https://swissmodel.expasy.org/interactive) with templates chosen based on highest sequence identity and coverage. Model quality was assessed using PROCHECK via the SAVES server (https://saves.mbi.ucla.edu/) and Ramachandran plot analysis was used to evaluate stereochemical reliability. The highest-quality models were saved in PDB format for subsequent molecular docking studies.

2.6.2. Ligand preparation of α-terpineol for molecular docking

The terpene compound α-terpineol, identified in the current study, was selected as the ligand for molecular docking analysis. The three-dimensional structure of α-terpineol in SDF format was retrieved from the PubChem database (https://pubchem.ncbi.nlm.nih.gov). Ligand preparation involved optimization of molecular geometry and calculation of key physicochemical properties, including molecular weight, net charge, and polar surface area. The ligand was maintained in its neutral form, and rotatable bonds were defined prior to docking.

2.6.3. Computational docking of APN– and ALP–ligand interactions

Molecular docking was carried out using AutoDock Vina v1.2.5 within PyRx v0.9.9 (https://pyrx.sourceforge.io/; accessed 20 November 2025) to evaluate interactions between α-terpineol and the modeled APN and ALP proteins. Blind docking was applied by defining a grid box covering the entire protein with a grid spacing of 1.0 Å. Ligands were prepared by adding Gasteiger charges, merging nonpolar hydrogens, and assigning rotatable bonds. Binding energies were estimated in kcal/mol, with lower values indicating stronger interactions. Docking poses were analyzed for hydrogen bonding and hydrophobic contacts, and molecular interactions were visualized using BIOVIA Discovery Studio Visualizer v24.1.0.23298 (Dassault Systèmes, France).

2.7. qRT–PCR analysis

For qRT-PCR analysis, total RNA was extracted from frozen leaf tissues of FAW-infested and uninfested maize samples (RP, RM, SP, and SM, $n = 12$) using the NucleoSpin RNA kit (MACHEREY-NAGEL, Germany) following the manufacturer's instructions. Purified RNA (2.0 μg) was reverse-transcribed into cDNA using the ThermoScript RT-PCR system (Invitrogen). Quantitative PCR was performed using gene-specific primers (Table S1, Fig. S2A), with two technical replications on a CFX96 Real-Time PCR system (Bio-Rad). Primer efficiencies were evaluated using standard curves and were within the acceptable range (90–110 %). Amplification specificity was verified by melt-curve analysis, which confirmed a single peak for each primer pair (Figure S2B). Ct values were normalized against the maize actin gene, and relative gene expression levels were calculated using the $2^{-\Delta\Delta Ct}$ method (Livak et al., 2001).

3. Results

3.1. Phenotypic reconfirmation of maize genotypes

The contrasting maize inbred lines, CML338 and CML451, were evaluated under controlled conditions for their response to fall armyworm (FAW) infestation. The resistant line, CML338, showed a lower leaf damage rating (4.8) than the susceptible line, CML451 (6.2) (Fig. S1).

3.2. Transcriptomics analysis of maize-faw interaction

High-quality clean reads were generated for all samples following filtering with Fastp (v0.23.2) using a Q30 threshold and a minimum read length of 70 bp, resulting in 92.6–94.7 % high-quality reads and GC content ranging from 50.5 to 55.2 %. The filtered reads were efficiently aligned to the *Zea mays* B73 reference genome using HISAT2, with the majority of samples exhibiting high mapping rates of 84–87 %, demonstrating strong compatibility between the sequencing data and the reference genome. Reference-guided assembly and quantification performed using StringTie (v2.1.4) yielded reliable transcript abundance estimates, which were normalized using FPKM (Fragments Per Kilobase of exon model per Million mapped reads) for accurate downstream gene expression analysis.

3.3. Multivariate analysis for RNA seq data

Differential expression and principal component analysis (PCA) performed using the DESeq2 R package revealed partial separation among RM, RP, SM, and SP groups. PC1 explained 36.8 % variance, discriminating between the resistant and the susceptible genotype. Each genotype formed its cluster of metabolites with a good overlap between the biological replicates. PC2 explained 23.7 % variance, discriminating FAW-fed from the unfed profile (Fig. 1A). In contrast, Partial Least Squares Discriminant Analysis (PLS-DA) achieved clear group separation, with Component 1 accounting for 61.2 % and Component 2 accounting for 38.8 % of the variance. This suggested minimal experimental error (Fig. 1B) and verified the results obtained through PCA by revealing noticeable differences between the samples under the mock treatment (RM and SM) and pest-infested treatment (RP and SP). Additionally, PLS-DA was performed using two latent components. The model explained 60.5 % of the total variance ($R^2 = 0.605$). Cross-validation (3-fold, 50 repeats) demonstrated strong predictive performance ($Q^2 = 0.917$) with a low classification error rate (7.3 %). Permutation testing (200 permutations) confirmed that the model performed significantly better than random classification ($p < 0.005$), indicating robust discrimination among experimental groups.

A four-way Venn diagram was constructed to evaluate the shared and unique differentially expressed genes (DEGs) across the four pairwise comparisons: RM vs SM, RP vs RM, SP vs SM, and RP vs SP. DEGs were defined based on Benjamini–Hochberg adjusted *p*-values (FDR $\leq$ 0.05) and $|\log_2 \text{fold change}| > 1.0$. The central intersection comprised 29,144 commonly regulated DEGs shared among all four comparisons, indicating a substantial core transcriptional response across conditions. Unique DEG subsets were identified in each contrast, including 53 (RM vs SM), 109 (RP vs RM), 159 (SP vs SM), and 55 (RP vs SP), reflecting condition-specific transcriptional modulation. Additional pairwise overlaps were observed, with 572 DEGs shared between RM vs SM and RP vs RM, and 967 between SP vs SM and RP vs SP (Fig. 1C), further illustrating both conserved and contrast-specific expression patterns.

In addition, correlation analysis revealed a high degree of consistency among biological replicates within each group, whereas significant differences were observed between replicates belonging to different sample groups (Fig. 1D). Differential expression analysis identified substantial transcriptional changes across the four pairwise comparisons when applying the cut-off of $\log_2$ (fold change) $\geq$ 1 and FDR $\leq$ 0.05. RP

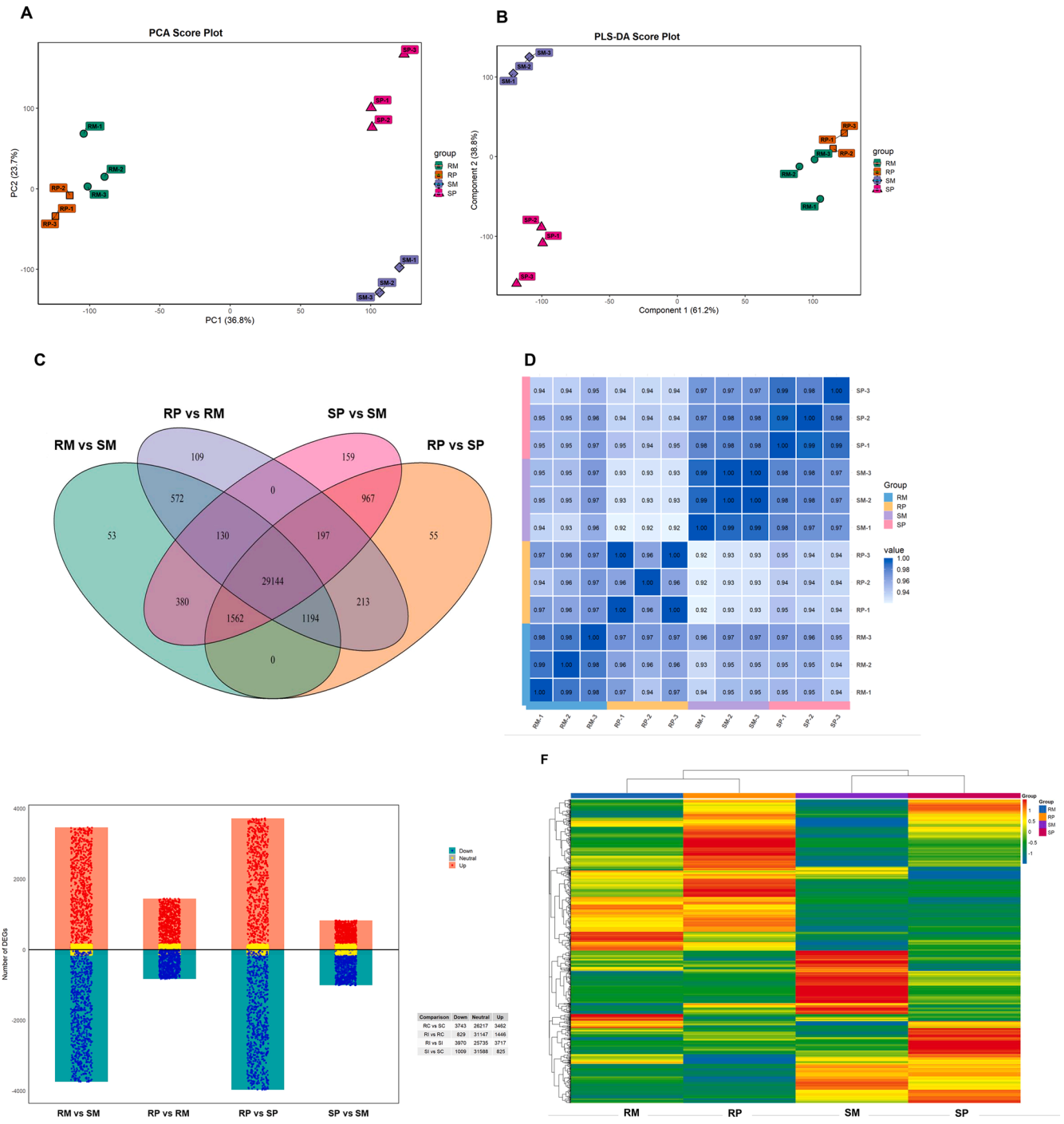


Fig. 1. Global transcriptome and differential gene expression (DEG) profiling of resistant and susceptible genotypes under pest stress. The analysis includes Resistant Mock (RM), Resistant Pest (RP), Susceptible Mock (SM), and Susceptible Pest (SP) samples. (A) Principal component analysis (PCA) score plot and (B) partial least squares discriminant analysis (PLS-DA) plot showing sample grouping under control and pest-stress conditions. (C) Venn diagrams illustrating unique and shared DEGs among treatments and genotypes. (D) Heatmap depicting the correlation of gene expression profiles among all biological replicates. (E) Volcano plots showing the distribution of DEGs in response to pest stress in resistant and susceptible genotypes. (F) Heatmap showing clustering of stress-responsive DEGs and (G) sub-clustering of DEGs based on log10(FPKM + 1) expression values.

vs SP comparison exhibited the highest number of differentially expressed genes (↑3717 and ↓3970), followed closely by RM vs SM (↑3462 and ↓3743), indicating pronounced transcriptional divergence under these conditions. In contrast, RP vs RM showed a more modest shift in gene expression (↑1446 and ↓829), while SP vs SM displayed the least number of DEGs (↑825 and ↓1009), suggesting relatively subtle molecular differences. These results highlight pronounced transcriptional divergence in RP vs SP and RM vs SM, whereas RP vs RM and SP vs SM exhibited comparatively fewer DEGs, reflecting more subtle molecular differences between those conditions (Fig. 1E).

Hierarchical clustering of the top 1000 significantly differentially expressed genes (DEGs; adjusted $p \leq 0.05$ and $|\log_2 FC| \geq 1$) revealed four major groups with similar expression patterns (Fig. 1F). Further, Z-score normalization was applied to standardize gene expression values

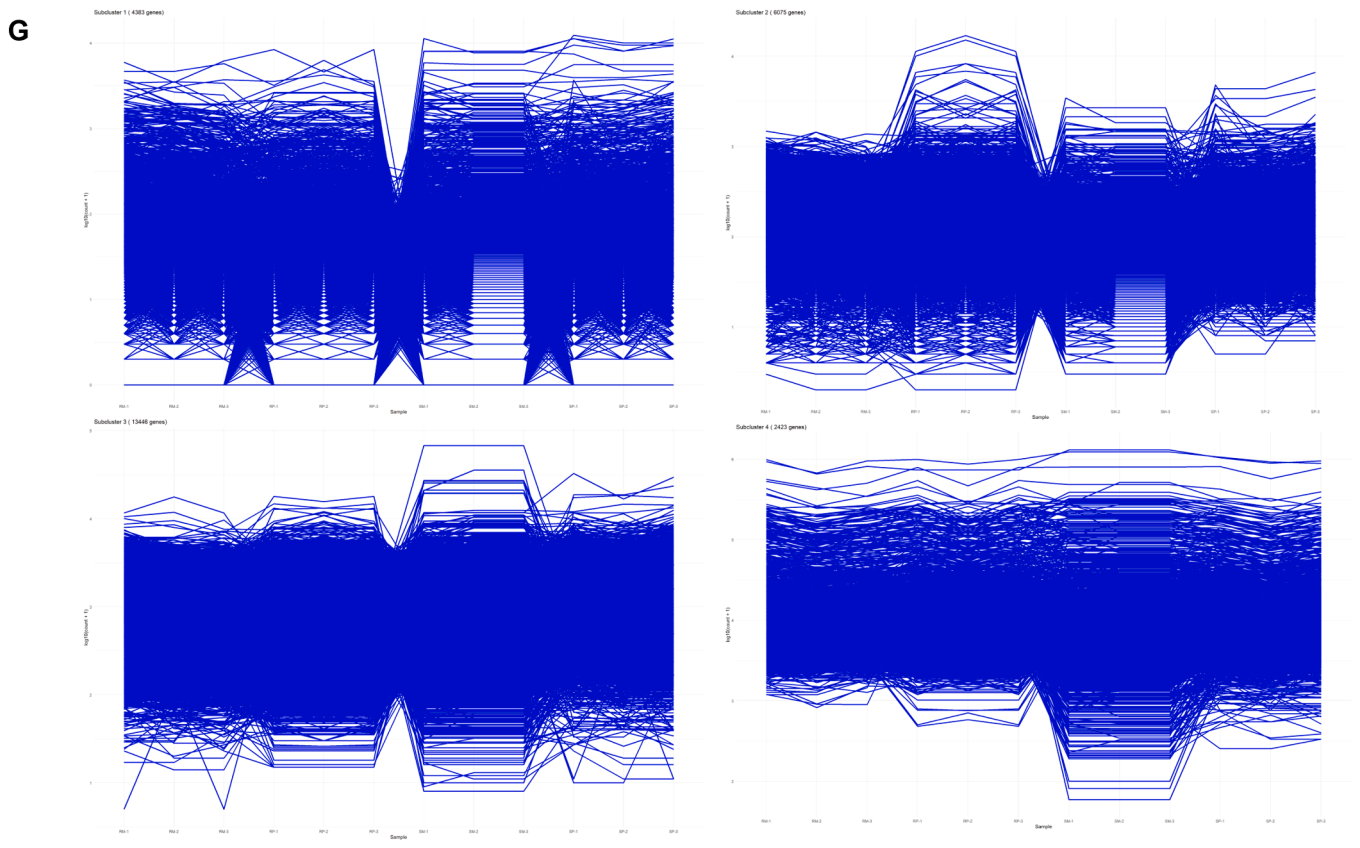


Fig. 1. (*continued*).

across samples, enabling clustering based on relative expression patterns rather than absolute expression levels. This facilitates clustering of genes that show similar responses across conditions, improving the interpretation of co-expression patterns. This analysis resolved four distinct subclusters: Subcluster 1 (4380 genes) showing consistent down-regulation over time, Subcluster 2 (6875 genes) exhibiting gradual upregulation, Subcluster 3 (5464 genes) displaying transient expression peaks at intermediate time points, and Subcluster 4 (3263 genes) with relatively stable or fluctuating expression patterns. These distinct clusters reflect coordinated and dynamic regulatory responses to the experimental conditions (Fig. 1G).

3.4. Differentially expressed gene identification enrichment analyses and pathway classification

3.4.1. Resistant-related constitutive (RRC) genes

All differentially expressed genes (DEGs) were functionally annotated across the three major Gene Ontology (GO) categories: Biological Process (BP) (associated with response to stimulus, metabolic process, and cellular regulation), Molecular Function (MF) (dominated by binding activity and catalytic functions), and Cellular Component (CC) (enriched with membrane-associated and intracellular organelle components) (Fig. 2A).

Complementary pathway enrichment analysis identified significantly over-represented pathways based on the Rich Factor and statistical significance ($-\log_{10} \geq 1$; $p \leq 0.05$). Notable enriched pathways included plant hormone signal transduction, MAPK signaling, and secondary metabolite biosynthesis, indicating that DEGs are involved in key regulatory and stress-responsive networks (Fig. 2B). However, the different classes and pathways associated with the RRC genes were analyzed based on their fold-change values (Table S2).

3.4.2. Resistant-related induced (RRI) genes

The GO terms by gene count, with catalytic activity, oxidoreductase activity, and membrane components among the top-enriched functions. These suggest active metabolic and redox processes, along with structural involvement in cellular compartments (Fig. 2C). Additionally, GO visualizing enrichment significance using Rich Factor and ($-\log_{10} \geq 1$; $p \leq 0.05$). Notably enriched terms include oxidoreductase activity, membrane part, and response to stimulus, indicating that the DEGs are functionally involved in stress response, enzymatic regulation, and membrane-associated processes. These findings provide insight into the biological roles and regulatory mechanisms influenced under the experimental conditions (Fig. 2D). However, the different classes and pathways associated with the RRI genes were analyzed based on their fold-change values (Table S3).

3.5. WGCNA reveals distinct transcriptomic networks associated with FAW resistance

WGCNA was performed on transcriptomic data derived from 12 samples, using the 10,000 most variable genes to construct the co-expression network. Evaluation of the scale-free topology fit index (R^2) across candidate soft-thresholding powers (1–20) indicated that $\beta = 20$ provided an optimal balance between scale-free topology ($R^2 \approx 0.8$) and network connectivity, and was therefore selected for construction of the adjacency and TOM. Hierarchical clustering combined with dynamic tree cutting and module merging at a cut height of 0.25 identified ten distinct gene co-expression modules, each represented by a unique color (Fig. 3A). Module sizes ranged from 66 genes (grey module) to 2802 genes (red module) (Fig. 3B). Module-trait correlation analysis revealed several modules significantly associated with FAW resistance after FDR correction (FDR < 0.05) (Fig. 3C). Among these, the red module exhibited the strongest positive association with the resistant phenotype ($r = 0.986$, FDR $= 3.8 \times 10^{-8}$). Robustness analyses further supported

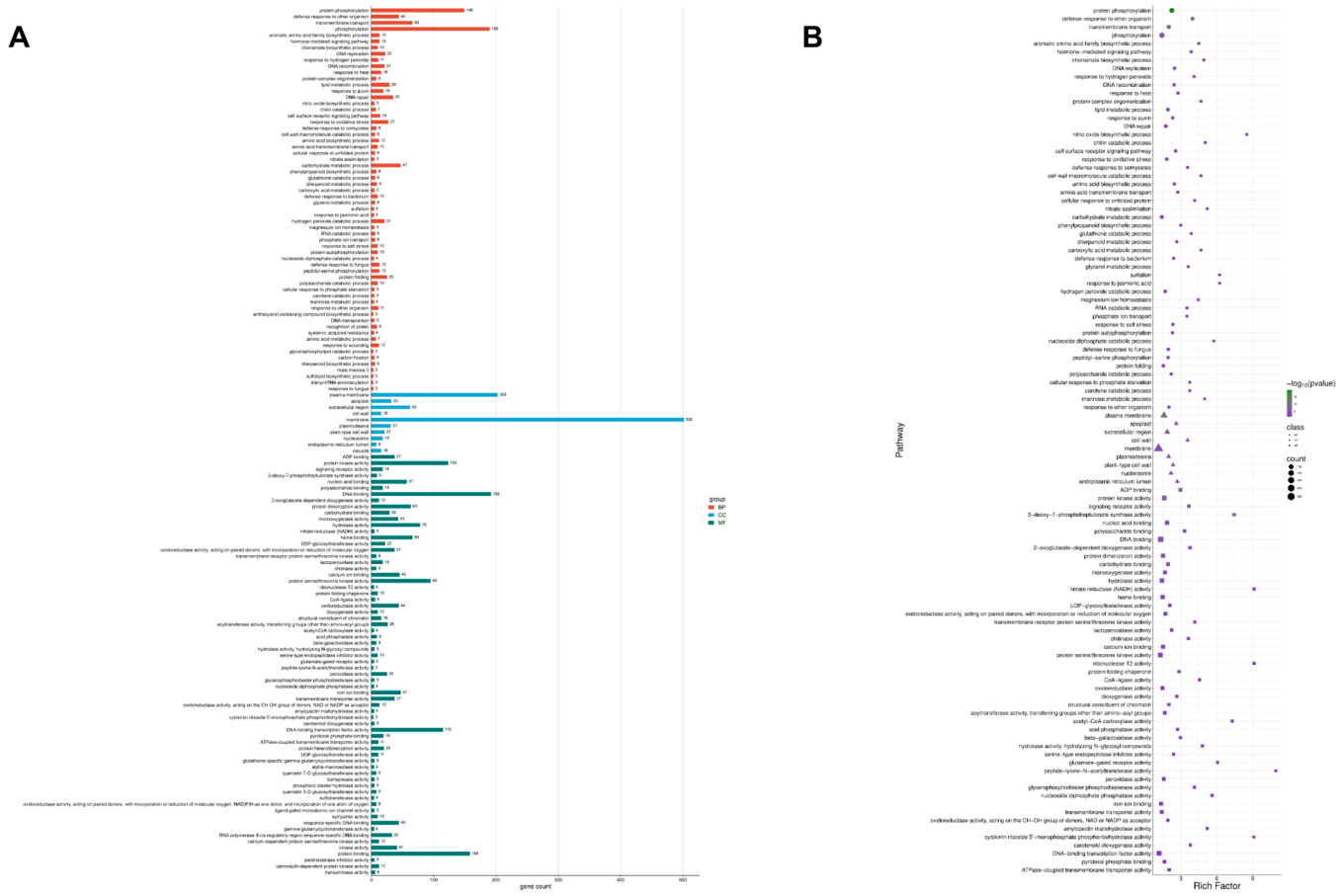


Fig. 2. Functional enrichment analysis of differentially expressed genes (DEGs) in resistant genotype comparisons. (A) Gene Ontology (GO) classification and (B) KEGG pathway enrichment bubble plot of DEGs in RRC. The size and color of the dots reflect gene count and enrichment significance, respectively, highlighting biologically relevant pathways impacted by the experimental conditions (C) Gene Ontology (GO) classification and (D) KEGG pathway enrichment bubble plot of DEGs in RRI and the larger dots indicate higher gene counts, while color intensity reflects statistical significance. Enriched terms and pathways were identified at a significance threshold of $P \leq 0.05$.

this association, as the correlation remained significant under 10,000 permutation tests ($P = 0.002$) and showed minimal variability during leave-one-out resampling (SD = 0.021), indicating that the observed relationship is stable and unlikely to be driven by individual samples (Fig. S3.). Network visualization of the red module (Fig. 3D) revealed dense co-expression among genes involved in calcium signaling, cell wall reinforcement, transcriptional regulation, receptor-mediated defense, phytohormone signaling, fatty acid metabolism, and flavonoid biosynthesis. These results suggest that the red module represents a central transcriptional regulatory network coordinating maize defense response against FAW. Given the moderate sample size, these strong correlations are interpreted as robust associations rather than direct causal relationships.

3.5.1. *Metabolomics analysis of maize-FAW interaction*

Metabolites were confirmed based on matching database with a mass accuracy within ±10 ppm. These metabolites were designated as resistance-related constitutive (RRC) metabolites (Table S4). The identified RRC metabolites were classified into distinct chemical groups to elucidate the biological pathways significantly altered under non-infested conditions in maize. In contrast, following FAW infestation, several metabolites showed a marked increase in abundance in the resistant genotype and were therefore designated as resistance-related induced (RRI) metabolites (Table S5).

3.5.2. *Multivariate analysis of metabolomics data*

Differential expression analysis was performed using the DESeq2 R package in which PCA revealed partial separation among RM, RP, SM, and SP groups. PC1 explained 45 % of the total variance, primarily distinguishing resistant (RM, RP) from susceptible (SM, SP) genotypes. Each genotype formed distinct clusters with minor overlap among biological replicates. PC2 accounted for 29.1 % of the variance, separating pest-infested samples (RP, SP) from mock-treated controls (RM, SM) (Fig. 4A). In contrast, PLS-DA achieved complete group separation, with Component 1 (60.7 %) and Component 2 (39.3 %) together capturing the full modeled variance, indicating minimal experimental noise (Fig. 4B). Additionally, cross-validation demonstrated strong predictive performance ($Q^2 = 0.664$). Permutation testing (200 permutations) confirmed that the model performed significantly better than random classification ($p < 0.005$), indicating robust and statistically supported discrimination among the experimental groups.

Additionally, based on PLS-DA analysis, the heatmap generated depicted the relative abundance of metabolites captured through VIP (Variable Importance in Projection) scores; higher VIP scores indicated stronger discriminatory power for compounds. Based on this, metabolites across RM, RP, SM, and SP groups were ranked. This analysis showed that metabolites predominantly enriched in RM and RP were associated with resistant genotypes, whereas metabolites more abundant in SM and SP were associated with susceptibility. The blue-to-red color gradient highlights differential metabolite accumulation across groups (Fig. 4C).

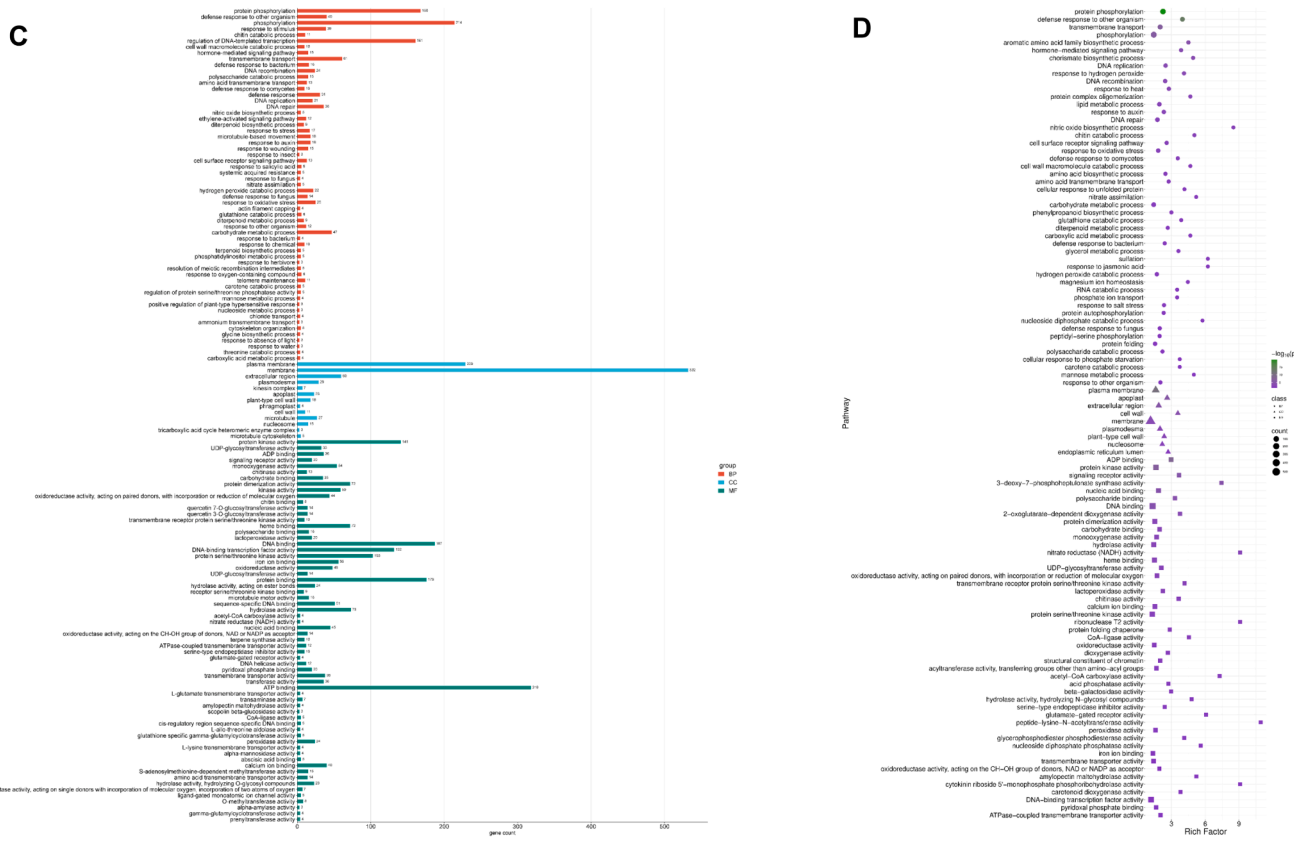


Fig. 2. (*continued*).

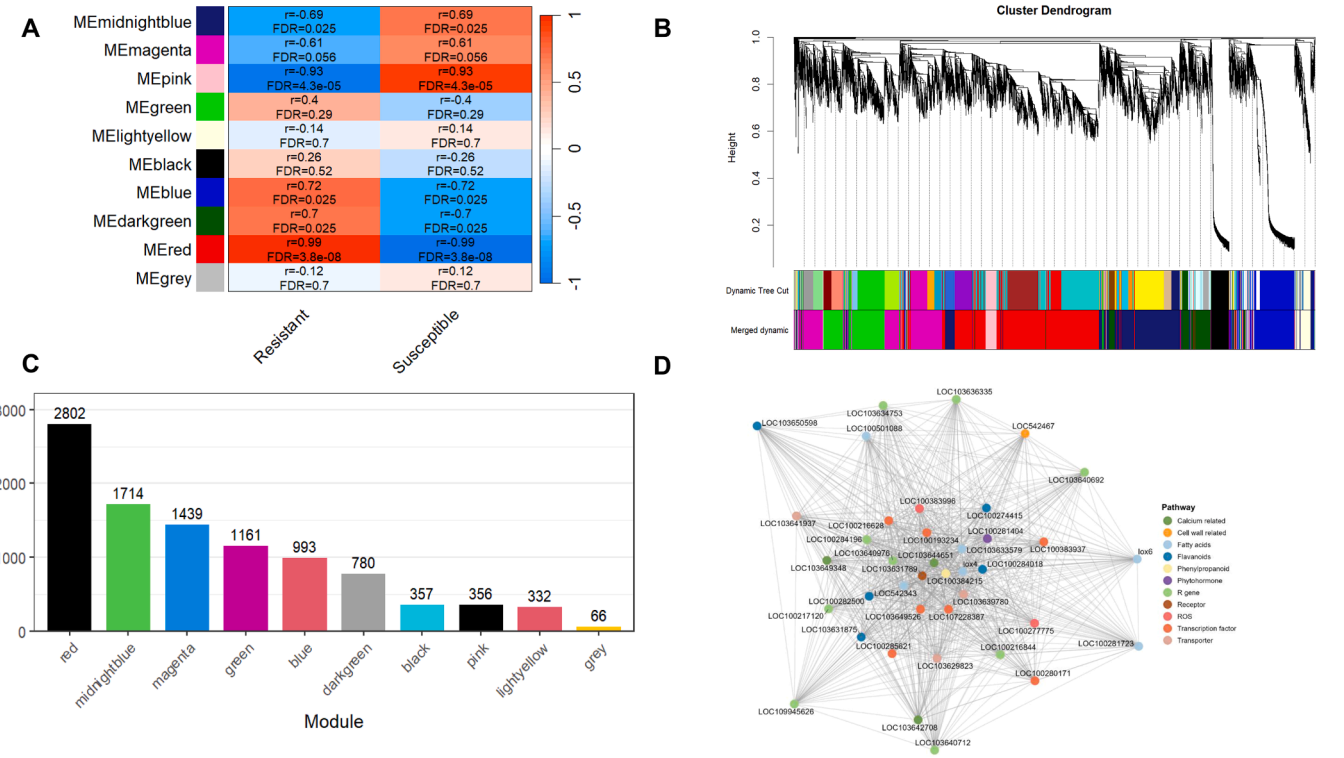


Fig. 3. Weighted Gene Co-expression Network Analysis (WGCNA) of transcriptome and differentially expressed gene's (DEGs) profiles from contrasting genotypes under pest stress. The analysis includes Resistant Mock (RM), Resistant Pest (RP), Susceptible Mock (SM), and Susceptible Pest (SP) samples.

A Venn diagram was constructed to assess the shared and unique features across differential comparisons: RP vs SP, RP vs RM, SP vs SM,

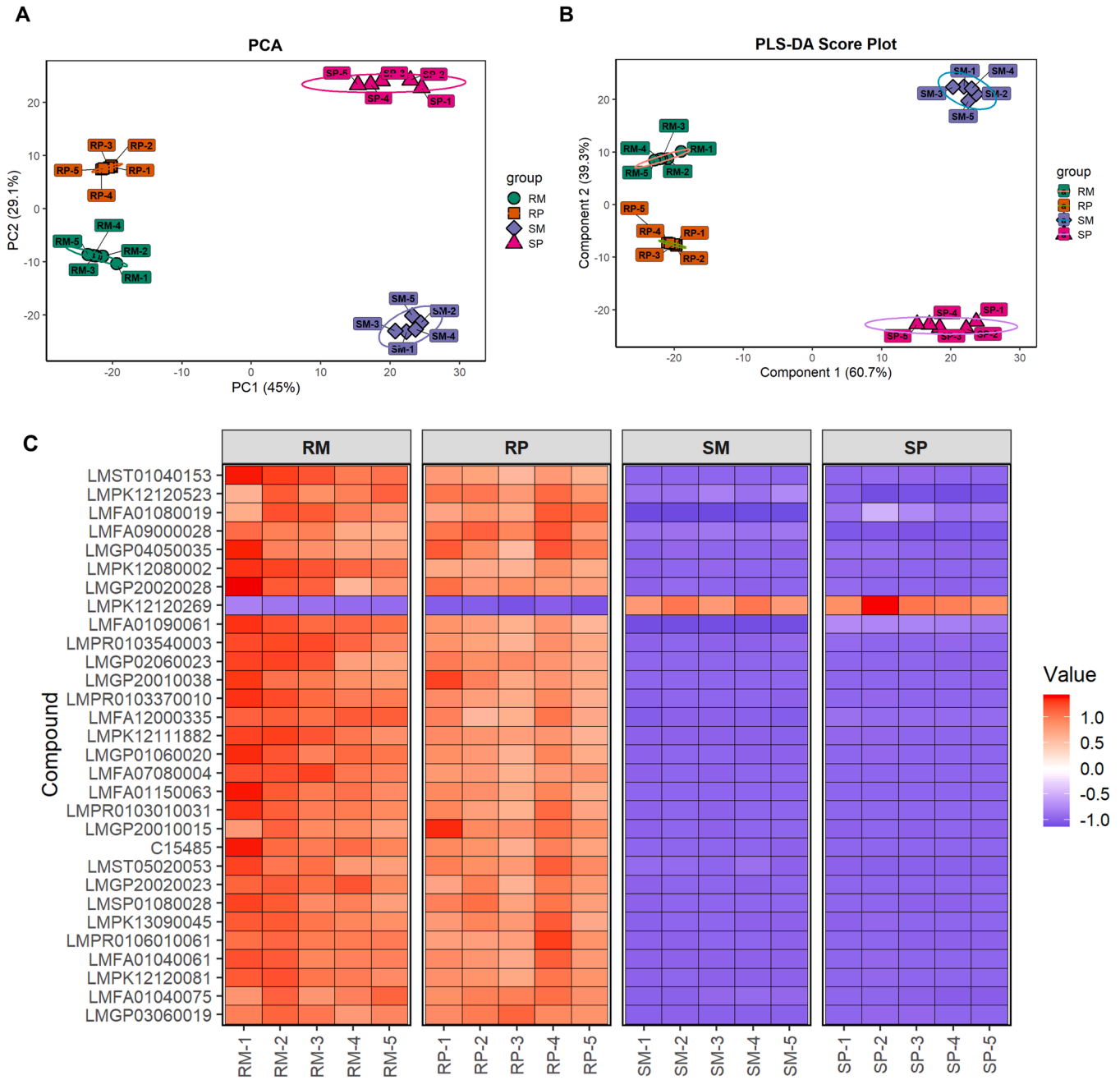


Fig. 4. Global metabolomic profiling and differential metabolite (DEM) analysis of contrasting genotypes under pest stress. The analysis includes Resistant Mock (RM), Resistant Pest (RP), Susceptible Mock (SM), and Susceptible Pest (SP) samples. (A) Principal component analysis (PCA) score plot and (B) partial least squares discriminant analysis (PLS-DA) plot of RP, RM, SP, and SM samples. (C) Variable importance in projection (VIP) scores of the top 20 significantly altered metabolites among the RP, RM, SP, and SM comparisons. (D) Venn diagrams showing unique and shared DEMs ($P \leq 0.05$). (E) Volcano plots displaying the distribution of DEMs for RP, RM, SP, and SM (FC ≥ 1; $P \leq 0.05$).

and RM vs SM. The central intersection revealed 268 common DEMs across all four comparisons, indicating a conserved core set. Unique subsets were observed in each contrast, including 49 (RP vs SP), 28 (RP vs RM), 9 (SP vs SM), and 8 (RM vs SM), highlighting condition-specific responses. Additional overlaps included 136 metabolites shared in RP vs SP and RP vs RM, 83 between RP vs SP, RP vs RM, and SP vs SM, and 127 among RP vs SP, RM vs SM, and RP vs RM (Fig. 4D).

The volcano plot of RP vs SP comparison exhibited the highest number of differentially accumulated metabolites (↑195 and ↓492), followed by RP vs RM (↑274 and ↓301), indicating strong metabolic shifts under pest-infested conditions. RM vs SM showed a moderate change (↑171 and ↓220), while SP vs SM displayed the least number of differentially accumulated metabolites (↑195 and ↓156), suggesting minimal perturbation in susceptible genotypes. Notably, RP vs SP and RP vs RM comparisons reflect pronounced condition-specific metabolic responses, whereas RM vs SM and SP vs SM likely represent baseline or transitional changes with limited impact (Fig. 4E).

3.6. *Metabolomics wgcna identifies coordinated defense-related metabolic modules*

WGCNA was performed on the metabolomics dataset consisting of 20

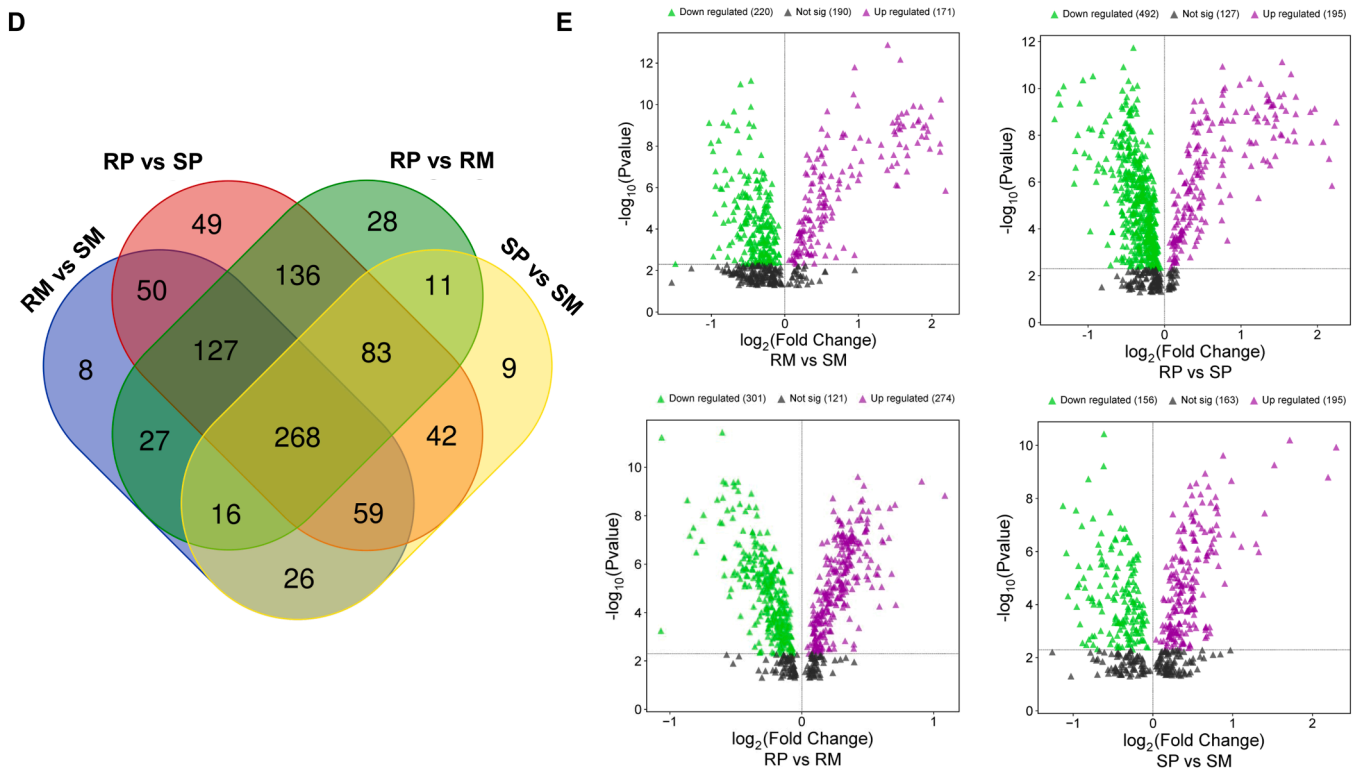


Fig. 4. (*continued*).

samples to identify coordinated metabolic modules associated with maize resistance to FAW. Evaluation of the scale-free topology fit index (R^2) across candidate soft-thresholding powers (1–20) indicated that $\beta = 20$ achieved an optimal balance between scale-free topology ($R^2 \approx 0.8$) and network connectivity and was therefore selected for construction of the adjacency and TOM. Hierarchical clustering of processed metabolite profiles followed by dynamic tree cutting and module merging at a cut height of 0.25 identified ten metabolite co-expression modules (Fig. 5A).

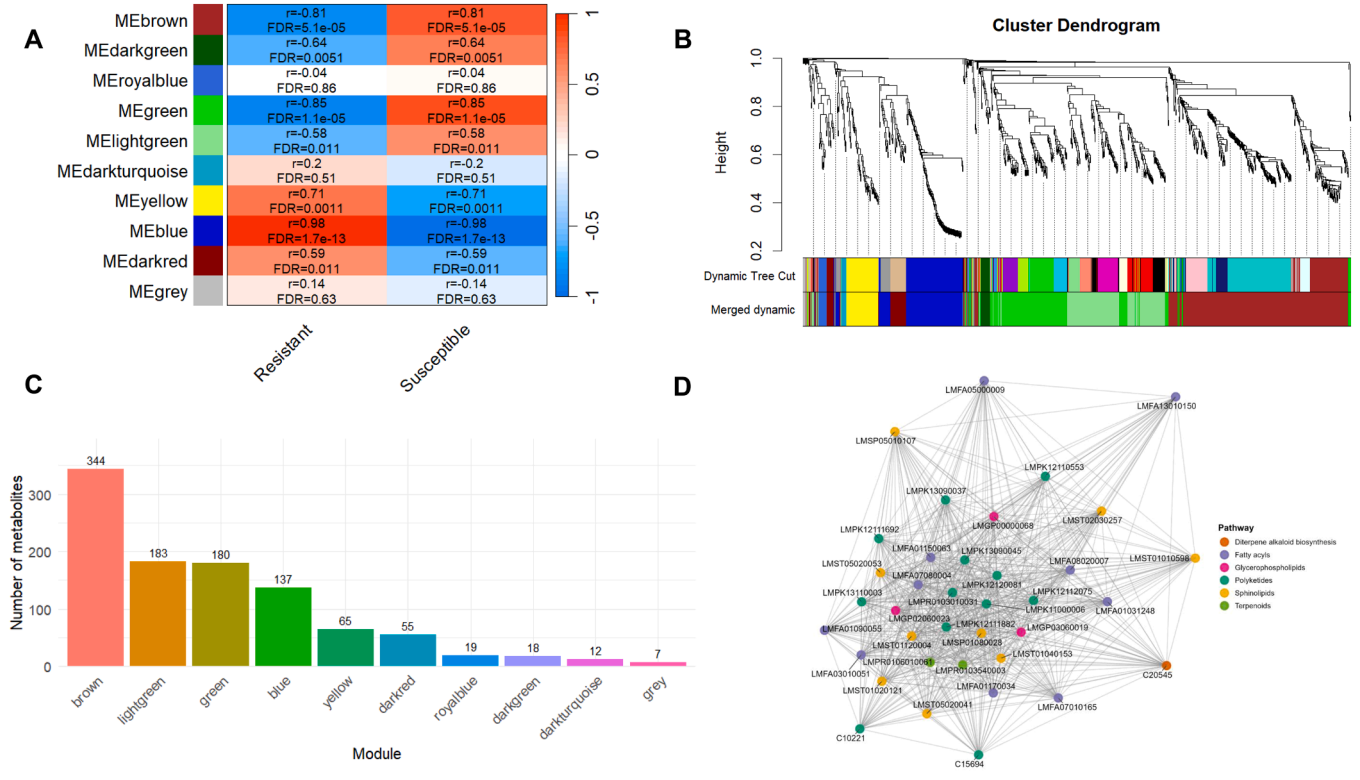


Fig. 5. Weighted correlation network analysis (WGCNA) of metabolomic profiles and differentially accumulated metabolites (DEMs) in contrasting genotypes under pest stress. The analysis includes Resistant Mock (RM), Resistant Pest (RP), Susceptible Mock (SM), and Susceptible Pest (SP) samples.

Module sizes ranged from 7 metabolites (grey module) to 344 metabolites (brown module) (Fig. 5B). Module–trait correlation analysis revealed several modules significantly associated with FAW resistance after FDR correction (FDR < 0.05) (Fig. 5C). Among these, the blue module showed the strongest positive association with the resistant phenotype ($r = 0.982$, FDR $= 1.65 \times 10^{-13}$). Robustness analyses further confirmed this association, as the correlation remained highly significant under 10,000 permutation tests ($P < 0.001$) and exhibited low variability during leave-one-out resampling (SD = 0.053), indicating stable module–trait relationships across samples (Fig. S4). Network analysis of the resistance-associated blue module (Fig. 5D) revealed tightly co-expressed metabolites, including fatty acyls, diterpene

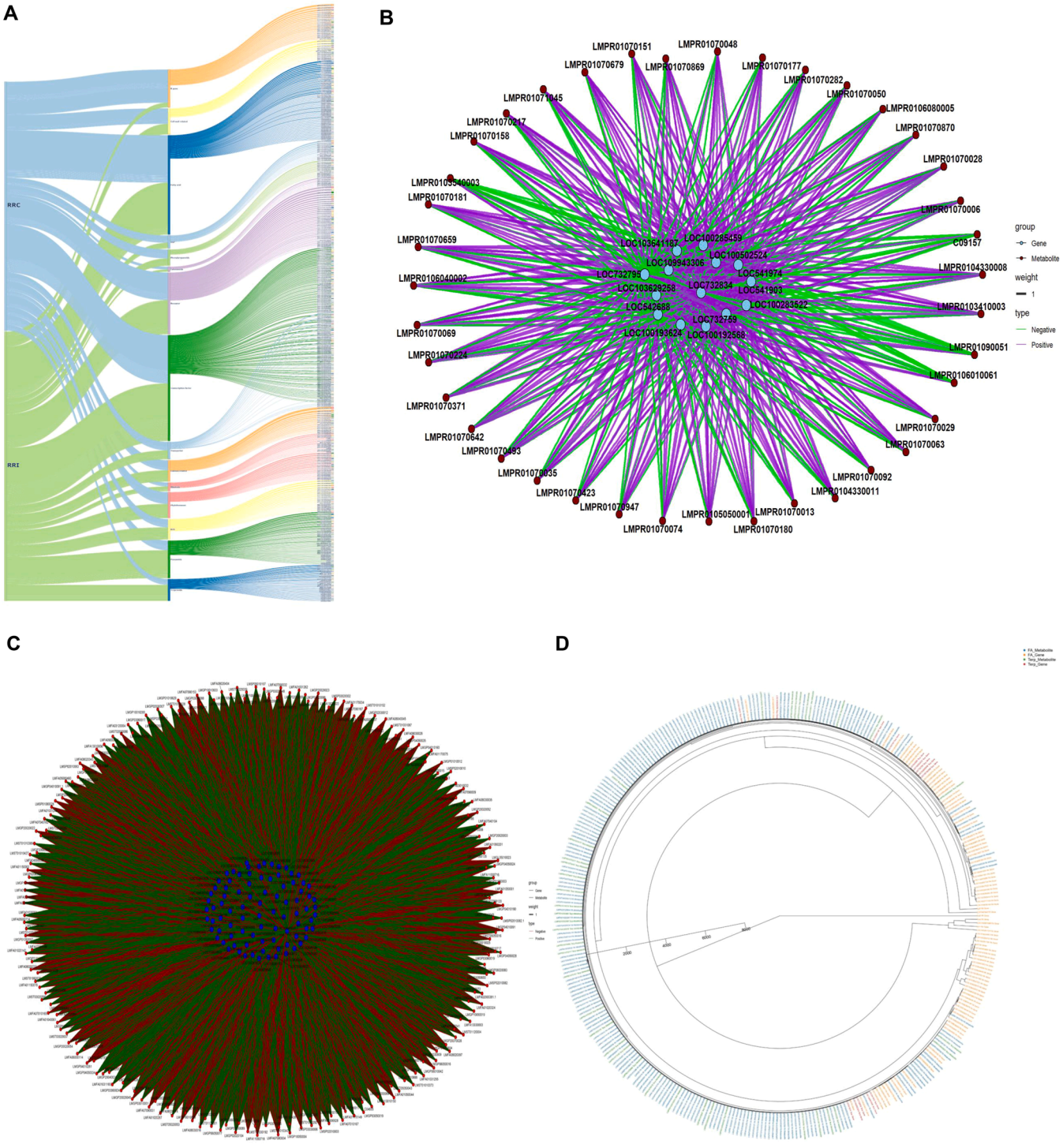


Fig. 6. Integrated transcriptomic and metabolomic analysis of maize resistance to fall armyworm (FAW). (A) Sankey diagram illustrating the metabolic linkages underlying resistance traits. Resistant-Related Compounds (RRC) and Resistant-Related Indicators (RRI) are linked to major metabolite classes, which further branch into specific defense-related compounds and their corresponding genes. The width of the flows represents the relative contribution, highlighting key pathways and metabolites involved in maize resistance to FAW. (B) Correlation network analysis of terpenoid-related differentially expressed genes (DEGs) and differentially accumulated metabolites (DEMs). (C) Correlation network analysis and (D) phylogenetic analysis of fatty acid–related DEGs and DEMs.

alkaloids, polyketides, and terpenoids—compound classes well known for their anti-herbivore and defensive functions. The strong co-expression patterns within this module indicate a coordinated metabolic defense system contributing to FAW resistance in maize.

3.7. Integrative analysis of transcriptome combined with metabolome

Integrated transcriptome–metabolome correlation analysis revealed coordinated gene regulation and metabolite accumulation underlying maize resistance to FAW, linking transcriptional changes to metabolic responses associated with resistance.

The Sankey plot illustrated the distribution of transcriptomic and metabolomic features across functional categories in RRC and RRI (Fig. 6A). Fatty acid metabolism showed high representation in both RRC (177) and RRI (194), while transcription factors were similarly abundant in RRC (157) and RRI (160), highlighting their central regulatory roles. Marked increases in RRI were observed for flavonoids (RRC: 21; RRI: 89) and terpenoids (RRC: 14; RRI: 44), indicating enhanced secondary metabolism under induced conditions. ROS-related features were moderately higher in RRI (29) than RRC (24), reflecting elevated oxidative stress responses. Several categories, including calcium signaling, transcription factors, and ROS, were shared between RRC and RRI but differed in abundance, underscoring distinct regulatory and defense responses between the two conditions.

Using PCC $\geq$ 0.85 and $P \leq 0.05$ (FDR $\leq$ 0.05) as screening criteria, significantly enriched metabolic pathways were identified, with plant hormone signal transduction being the predominant pathway which includes the fatty acid pathway and terpenoid pathways. The correlation network analysis revealed coordinated regulation of terpenoid and fatty acid metabolism during the maize response to FAW infestation. In the terpenoid network (Fig. 6B), both positive and negative correlations were detected between terpenoid-related DEGs and DEMs, indicating coordinated biosynthesis as well as feedback regulation within the pathway. Several gene–metabolite pairs showed strong positive associations, suggesting synchronized gene expression and metabolite accumulation, whereas negatively correlated pairs indicated regulatory mechanisms that may balance metabolic flux. The presence of hub genes and metabolites with multiple connections highlights key regulatory components of terpenoid biosynthesis. In the fatty acid network (Fig. 6C), extensive and dense interactions between fatty acid–related DEGs and DEMs were observed, reflecting tight transcriptional–metabolic coordination. The coexistence of positive and negative correlations indicates complex regulation of fatty acid metabolism under FAW stress. Phylogenetic analysis of fatty acid–associated DEGs (Fig. 6D) grouped these genes into distinct clades, revealing both functional diversification and conservation of core biosynthetic and signaling genes, supporting their central role in maize defense against FAW.

The RRC metabolites were classified into different chemical groups to identify the biological pathways that were significantly altered following treatment with FAW infestation (Table 1). Metabolomic analysis revealed that several fatty acids and terpenoids were distinctly expressed in resistant maize lines compared to susceptible ones. Among the fatty acids, linoleic acid showed the highest fold change (FC = 3.58) and was significantly associated with RRC. Moreover, arachidonic acid exhibited a fold change of 2.96 and was present in RRI, while hydroxyphthioceranic acid was expressed in both RRC (FC = 2.25) and RRI (FC = 2.94). Additionally, thalassotalic acid and arachidyl oleate contributed to resistance (Table 1).

Among the terpenoids, 5-hydroxyzeaxanthin showed up in RRI. Similarly, stelleracin (FC = 2.49), capsorubin (FC = 2.12), and pectenol A (FC = 2.12) specifically induced the resistance in maize RRI, suggesting their involvement in induced resistance responses. Lower yet significant fold changes were observed in violaxanthin (FC = 1.16), (-)-helvolic acid (FC = 1.08), and matricin (FC = 1.02), all contributing as RRI compounds (Table 1; Table S6).

Table 1
Putative resistance-related fatty acid- and terpenoid-associated metabolites detected in maize leaves following FAW or mock infestation. Fragmentation details for these metabolites are provided in Table S6.

Observed mass (Da)	Exact mass (Da)	Metabolite name	Fold change (FC)	
			RRC	RRI
Fatty Acids				
282.15	282.15	3,4-dimethyl-5-carboxypropyl-2-furanpentanoic acid	129.58**	
350.19	350.19	Methyl 9-(alpha-D-galactosyloxy)nonanoate		123.87**
414.22	414.23	Methyl 5-hydroperoxy-6,8,9,11-bisepidioxy-12,14-eicosadienoate	66.41**	
529.23	529.23	Lauroyl adenylate	64.38**	
432.25	432.25	Heterofibrin B3	36.35**	
432.27	432.26	1-(11,12-Methyleneoctadecanoyl)-sn-glycero-2,3-cyclic phosphate	32.56**	
185.07	185.07	N-(3-oxo-butanoyl)-homoserine lactone	9.81**	
244.20	244.20	Alpha-hydroxy myristic acid	8.60**	1.13**
296.24	296.24	13-keto-9Z-octadecenoic acid	6.60**	2.06**
404.24	404.23	1-(9,10-Methylenehexadecanoyl)-sn-glycero-2,3-cyclic phosphate		4.70**
244.20	244.20	Omega-hydroxy myristic acid	3.77**	
227.15	227.15	N-octanoyl-homoserine lactone	3.63**	4.58**
284.26	284.27	Linoleic acid(d4)	3.58**	
282.13	282.13	R-Protegenin B	3.39**	
334.22	334.21	5Z,8Z,11Z,14Z-Eicosatetraenedioic acid	3.33**	
292.21	292.20	7-Hydroxy-octadeca-7Z,9Z-dien-5-ynoic acid		3.23**
317.27	317.27	N-methyl arachidonoyl amine	3.17**	
242.23	242.22	2-methyl-tetradecanoic acid	3.16**	
294.14	294.14	Ginsenoyne B	3.05**	
304.24	304.24	Arachidonic acid		2.96**
334.22	334.21	15-deoxy-delta-12,14-PGD2	2.89**	
407.27	407.27	N-linolenoyl glutamic acid		2.50**
255.16	255.16	Albanitrile E		2.32**
273.24	273.25	10Z,13Z,16Z-nonadecatrienenitrile	2.29**	
566.56	566.56	Hydroxyphthioceranic acid (C37)	2.25**	2.94**
620.45	620.45	N-lignoceroyl-O-phosphocholineserine		2.22**
296.15	296.15	Panaxydol chlorohydrine	2.07**	
608.38	608.38	Dokdolipid C		2.07**
268.24	268.24	14R-methyl-8Z-hexadecenoic acid	2.00**	2.12**
588.43	588.42	3-O-alpha-L-rhamnopyranosyl-3-hydroxypalmitoyl-3-hydroxydecanoic acid		1.89**
563.50	563.50	N-(4-isobutyramidobutyl)-15-methyl-N-(4-pentanamidobutyl) hexadec-6E-enamide	1.86**	
334.23	334.23	9-chloro-10-hydroxy-octadecanoic acid	1.70**	
333.19	333.19	Thalassotalic acid A		1.69**
360.24	360.24	1-dimethylarsinoyl-heptadecane		1.68**
285.27	285.27	Pentadecanoyl-EA	1.65**	
562.57	562.57	Arachidyl oleate	1.62**	
532.36	532.36	3-O-alpha-L-rhamnopyranosyl-3-hydroxydodecanoyl-3-hydroxydecanoic acid		1.57**
310.32	310.32	6Z-Heneicosen-11-ol	1.43**	1.48**
564.39	564.39	N-arachidoyl-O-phosphocholineserine		1.43**

(continued on next page)

Table 1 (*continued*)

Observed mass (Da)	Exact mass (Da)	Metabolite name	Fold change (FC)	
			RRC	RRI
476.28	476.28	Solacetal A	1.42**	1.07**
587.42	587.42	Melonosin B		1.41**
468.36	468.36	(-)-Petrosynoic acid A		1.31**
374.25	374.25	1-dimethylarsinoyl-octadecane	1.27**	
294.22	294.22	5-keto-6E,8E-octadecadienoic acid		1.26**
281.17	281.17	N-octanoyl histidine		1.25**
506.28	506.27	(3b,9R)-5-Megastigmene-3,9-diol 9-[apiosyl-(1->6)-glucoside]		1.23**
279.18	279.18	N-(2E,4E-dodecadienoyl)-homoserine lactone		1.08**
334.20	334.20	3—O-alpha-L-rhamnopyranosyl-3-hydroxydecanoic acid		1.08**
165.99	165.99	Alpha-T		1.04**
353.26	353.26	N-(3-oxo-hexadecanoyl)-homoserine lactone		1.01**
568.31	568.30	Helvolic acid		27.51**
558.48	558.48	1—Hydroxy-zeta-carotene	3.07**	4.99**
586.43	586.44	5-Hydroxyzeaxanthin		3.53**
570.44	570.44	1,1′-(OH)2–3,4-Didehydrolycopene		3.03**
568.43	568.43	Tunaxanthin E		2.76**
568.42	568.43	meso-Zeaxanthin/ (3R,3′S)-Zeaxanthin		2.73**
570.44	570.44	Parasiloxanthin/ 7,8-Dihydrozeaxanthin		2.68**
568.43	568.43	Lutein F		2.68**
620.33	620.33	Stelleracin A		2.49**
552.43	552.43	1-OH-3′,4′-Didehydrolycopene		2.33**
568.43	568.43	2,2′-Dihydroxy-beta-carotene		2.20**
1166.95	1166.95	Mactraxanthin 3-gondoate 3′-palmitate		2.20**
608.29	608.30	Dapholosericin A		2.13**
582.40	582.41	Pectenol A		2.12**
600.41	600.42	Capsorubin		2.12**
586.44	586.44	OH-Demethylspheroidenone		2.03**
598.41	598.40	Halocynthiaxanthin		1.99**
600.45	600.45	R.g.Keto-IV		1.90**
600.42	600.42	Cycloviolaxanthin		1.83**
598.41	598.40	4,4′-Dihydroxydiatoxanthin		1.79**
600.45	600.45	OH-Spheroidenone		1.72**
586.38	586.38	3-Ethanoyloxyisorenieratene		1.67**
582.39	582.39	OH-Diaponeurosporene glucoside ester		1.66**
636.44	636.44	Mactraxanthin		1.58**
582.37	582.37	2-Norastaxanthin		1.55**
550.42	550.42	1-OH-3,4,3′,4′-Tetradehydrolycopene		1.45**
582.37	582.37	3,4-Diketo-2′,3′-dihydroxy-2-nor-beta-carotene		1.41**
600.41	600.42	Capsanthin 3,6-epoxide		1.25**
600.42	600.42	Siphonaxanthin		1.23**
582.41	582.41	alpha-Doradexanthin/ (3S,3′S,6′R)-4-Ketolutein		1.20**
476.24	476.24	1-O-all-trans-retinoyl-beta-glucuronic acid	2.16**	1.16**
600.42	600.42	Violaxanthin		1.16**
614.43	614.43	19-Methoxy siphonaxanthin		1.13**
400.26	400.26	Ophiobolin A		1.12**
568.34	568.34	(-)-Helvolic acid		1.08**
306.15	306.15	Matricin		1.02**

** p values $\leq$ 0.05.

3.8. *In-Silico 3D modeling and molecular docking reveal preferential binding site of α-Terpineol to target sites of FAW gut enzymes*

Molecular docking analysis demonstrated that α-terpineol interacts with multiple target enzymes, exhibiting distinct binding affinities and residue-specific interactions. Among the proteins tested, α-terpineol showed putative binding to Aminopeptidase N1, followed by Aminopeptidase N, Aminopeptidase N2, and Alkaline Phosphatase.

α-Terpineol bound to Aminopeptidase N with a binding affinity of −6.1 kcal/mol (Fig. 7A), stabilized by hydrophobic and polar interactions involving residues VAL A:681, PHE A:677, GLN A:678, ALA A:718, GLN A:717, LYS A:756, GLY A:666, ARG A:667, ASP A:663, ILE A:662, and PHE A:714, with hydrogen bonding to GLN residues enhancing binding specificity. The strongest interaction was observed with Aminopeptidase N1, showing a binding affinity of −6.6 kcal/mol (Fig. 7B). This complex was stabilized by hydrogen bonds and hydrophobic contacts involving ARG A:415, PHE A:367, LYS A:364, and TYR A:348, resulting in deep ligand accommodation within the binding pocket. Docking with Aminopeptidase N2, yielded a moderate affinity of −5.4 kcal/mol (Fig. 7C), with interactions involving HIS A:342, ILE A:339, ARG A:338, GLU A:372, ASN A:369, TYR A:427, GLN A:428, and ALA A:424, suggesting reduced stabilization relative to N and N1. The weakest binding was observed with Alkaline Phosphatase, with an affinity of −5.1 kcal/mol, mediated by residues ARG A:262, ARG A:266, TYR A:225, and PRO A:221 (Fig. 7D). However, this represents a putative prediction based on computational evidence of potential metabolite–protein interactions, and further biochemical and bioassay validation is required for definitive confirmation.

3.8. *Differentially expressed genes in response to FAW infestation*

qRT-PCR analysis was performed to evaluate the expression changes of selected candidate genes from the fatty acid, flavonoid and terpenoid pathway in resistant and susceptible genotypes following FAW infestation or uninfestion (Fig. 8). Upon FAW feeding, Anthranilic Acid Methyltransferase 1 (AAMT1; 3.44-fold), Phospholipase D (PLD; 4.36-fold), Terpene Synthase (TPS; 8.75-fold), and Dihydroflavonol-4-reductase–like (DFR; 12.13-fold) genes showed significant upregulation in the resistant genotype compared with the susceptible genotype. In contrast, S-norcoclaurine synthase 2 (NCS-2) exhibited significant downregulation (–4.27-fold), while the Phosphate Transporter (PHT) gene displayed genotype-specific differential expression. Overall, the qRT-PCR results showed strong concordance with the transcriptomic data (Fig. 8), confirming distinct and gene-specific expression patterns between the resistant and susceptible genotypes in response to FAW feeding.

4. Discussion

4.1. *Maize phenotypic response to FAW*

Plant–herbivore interactions involve complex defense mechanisms (War et al., 2012). FAW, a recently invasive pest, severely threatens maize production by feeding on inner leaf whorls, particularly in young plants. Resistance is commonly evaluated at the V5–V6 stage using a 1–9 leaf damage rating scale (Soujanya et al., 2022). Native FAW resistance in maize is typically polygenic and partial (scores 3–5), whereas transgenic lines often show stronger resistance (scores 1–2) (Prasanna et al., 2018). Our no-choice feeding assay reconfirmed the resistant (CML338) (Matova et al., 2022) and susceptible (CML451) nature of the genotypes which were subsequently used for integrated transcriptomic and metabolomic analyses to elucidate defense mechanisms.

4.2. *Molecular mechanism involved in maize-faw defense mechanism and regulatory roles of receptors, transcription factors, ca-related and phytohormones*

Plants rapidly perceive herbivore attack and activate early defense responses involving ion fluxes, membrane depolarization, MAPK activation, reactive oxygen species (ROS), nitric oxide (NO), and phytohormone signaling (Dhanyakumar et al., 2026; Kolanchi et al., 2025).

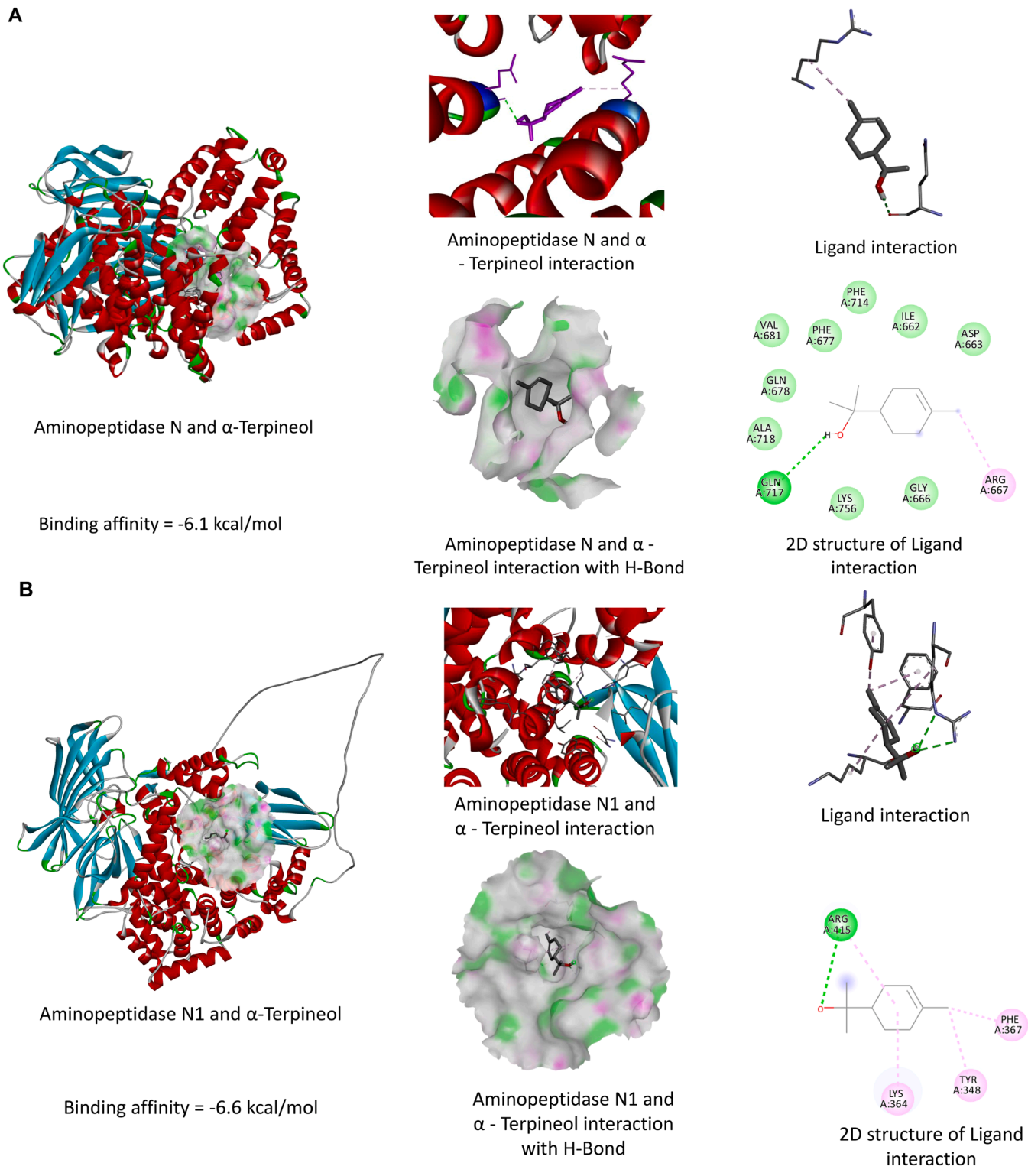


Fig. 7. Molecular docking analysis of α-terpineol with four target enzymes. The panels display ribbon and surface representations of the protein–ligand complexes, magnified views of the binding pockets, and two-dimensional (2D) interaction diagrams highlighting key amino acid residues involved in ligand binding. Subpanels show the interactions of α-terpineol with (A) Aminopeptidase N, (B) Aminopeptidase N1, (C) Aminopeptidase N2, and (D) Alkaline Phosphatase. The comparative visualization illustrates differences in ligand orientation, binding pocket architecture, and residue-level interactions among the four enzymes.

4.3. Receptor-like kinases

When an insect starts feeding on a plant, the plant recognizes herbivory-associated molecular patterns (HAMPs) and other signals through pattern recognition receptors (PRRs) (Malik et al., 2021). In our study, we observed the upregulation of several receptor-like kinase (RLK) families, including leucine-rich repeat (LRR), receptor-like cytoplasmic kinases (RLCKs), serine/threonine-protein phosphatase

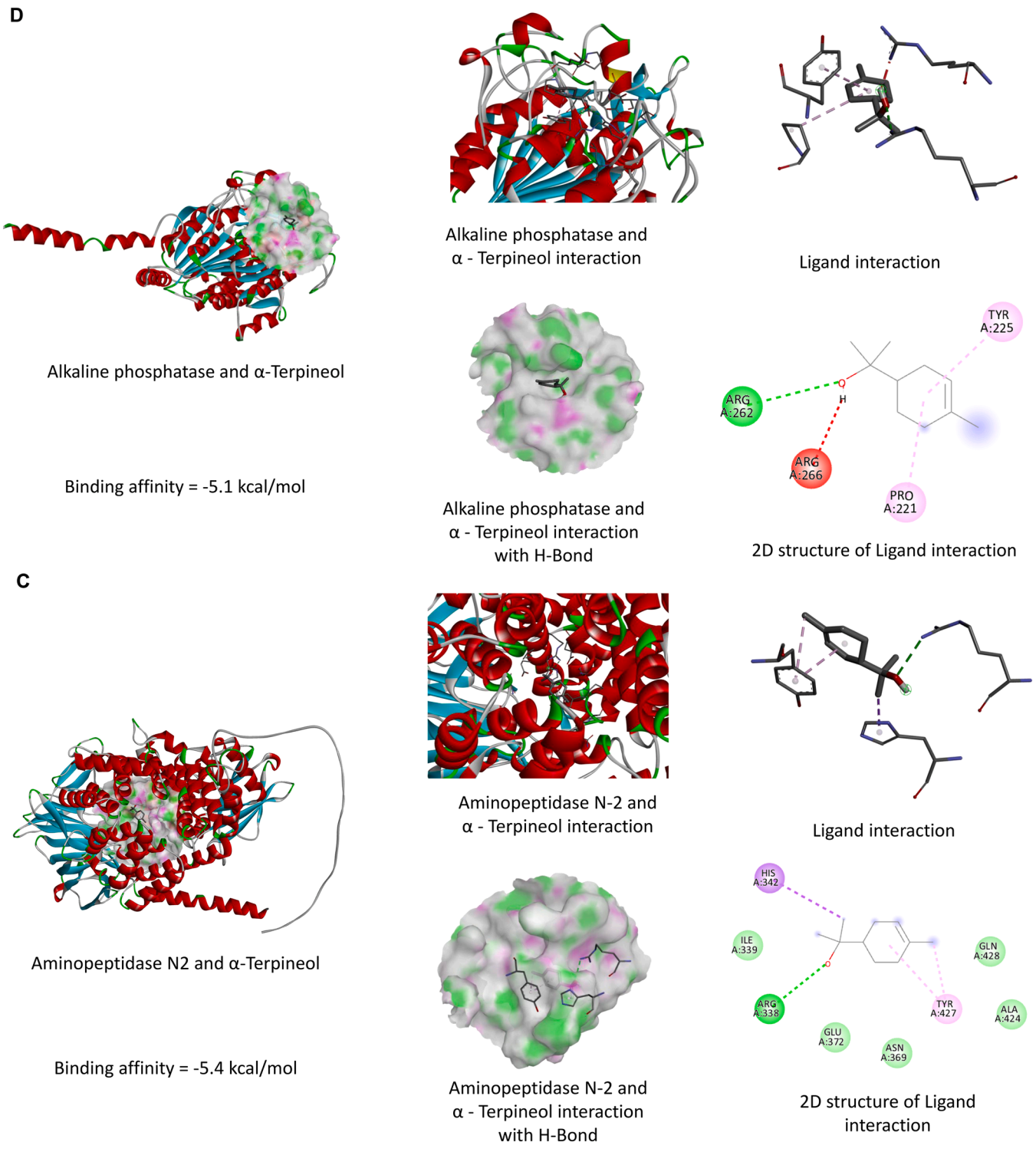


Fig. 7. (*continued*).

(Ser/Thr PP), PP1-like, and cysteine-rich receptor-like kinases (CRKs), in the resistant genotype following FAW infestation. Similar RLKs (*OsLRR-RLK1*) have been reported to respond to *Chilo suppressalis* (Hu et al., 2018) and *OsLRR-RLK2* by brown planthopper (*Nilaparvata lugens*) (Ye et al., 2020) feeding in rice. RLKs and receptor-like proteins function as PRRs that detect damage-associated and pathogen-associated molecular patterns, triggering ROS bursts, MAPK activation, and pattern-triggered immunity (PTI) (Wang et al., 2019; Tang et al., 2017).

Consistently, transcripts for MAPK signaling components, including MAPK9, MAPK16, MAPKK5, and MAPKKK17, were upregulated in RRI, suggesting activation of downstream defense pathways and phytohormone-mediated responses (Bricchi et al., 2012; Erb et al., 2012; Soltabayeva et al., 2022; Wu et al., 2010).

4.4. Calcium signaling

Calcium signaling is an important early defense response involving Ca^{2+} fluxes, calmodulins (CaMs), calmodulin-like proteins (CMLs), and

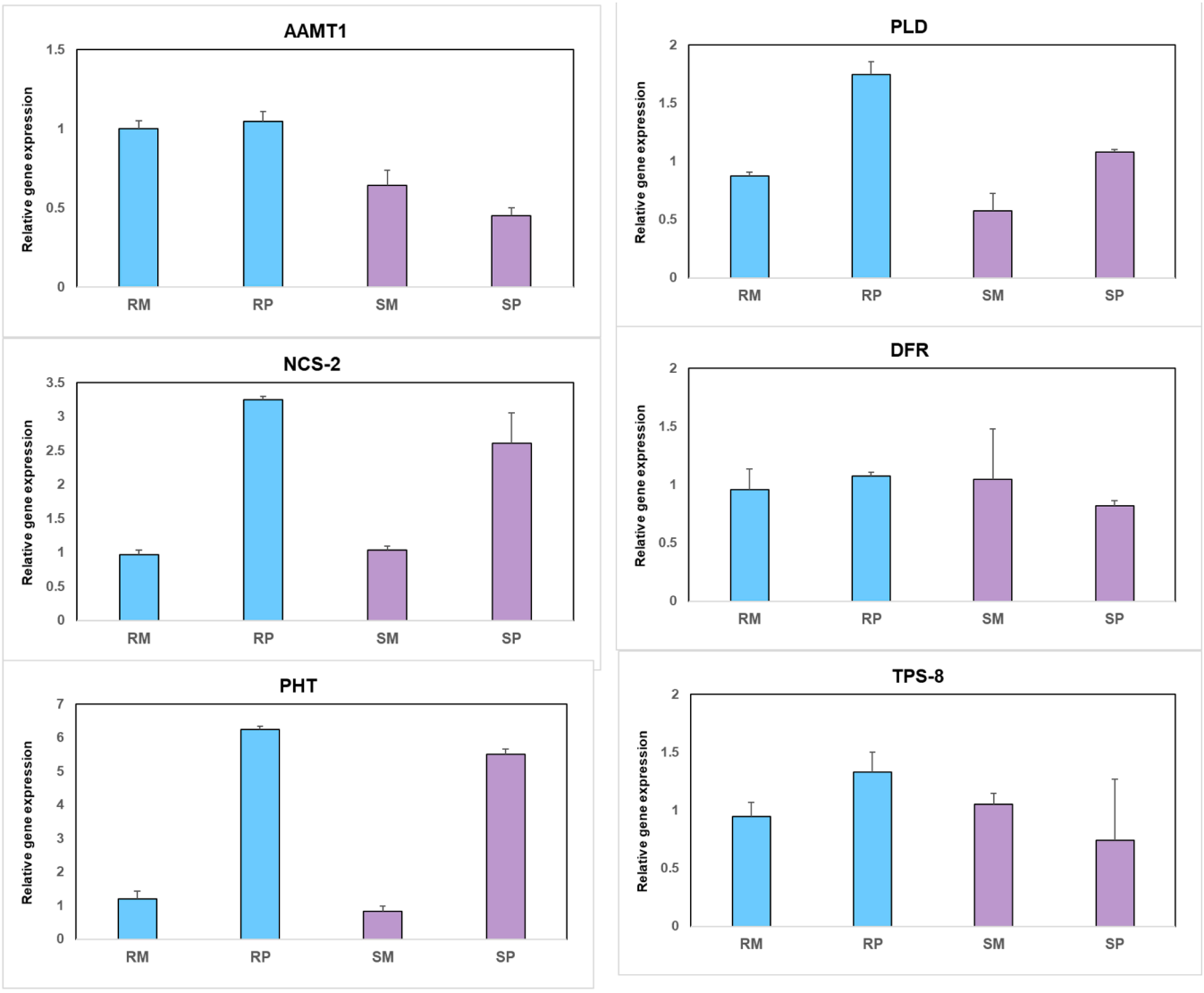


Fig. 8. Relative transcript expression of selected genes in resistant and susceptible maize genotypes under fall armyworm (FAW) infestation. Gene expression levels were analyzed by qRT–PCR at 48 h after infestation in both FAW-infested and uninfested (control) plants, normalized to the reference gene actin, and expressed relative to the susceptible genotype.

calcium-dependent protein kinases (CDPKs) (Fichman et al., 2020; Reddy et al., 2011). In this study, CDPK5, CDPK9, CDPK11, CDPK22, CaMs, and CMLs were identified, with CDPK9 and CDPK11 present under both constitutive and induced resistance conditions. CDPKs act as Ca^{2+} sensors and signal transducers, regulating defense responses to insect herbivory (Kanchiswamy et al., 2010). Previous studies show that in transgenic *Nicotiana attenuata* plants with silenced CDPKs, feeding by *Manduca sexta* larvae triggered elevated levels of defense-related metabolites that hindered larval growth. This underscores the essential role of CDPKs in regulating phytohormone homeostasis, highlighting the intricate interplay between phytohormones and MAPK signaling pathways (Yang et al., 2012). Similarly, in soybean, the expression of CDPK genes was altered by mechanical wounding and showed distinct patterns in response to simulated *Spodoptera exigua* feeding and *Aphis glycines* herbivory, indicating a significant role of CDPKs in mediating soybean–insect interactions (Hettenhausen et al., 2016).

4.5. *Transcription factors and phytohormone-related genes*

Upon encountering external stimuli, plants initiate several downstream signaling cascades that integrate transcriptional regulation and phytohormonal interactions. Herbivore attack rapidly activates transcription factors (TFs) that regulate defense gene expression (Schweizer et al., 2013). Key TFs include the WRKYs, MYB, NAC, MYC, ERF, and several others, which play a significant role in plant biotic stress responses (Birkenbihl et al., 2017; Fernández-Calvo et al., 2011). In our study, we observed the upregulation of TFs such as WRKY24, WRKY28, WRKY62, WRKY70, WRKY72 and MYB family includes MYB 2, MYB6, MYB29 MYB44, MYB77, and MYB108, and MYC family transcription factor such as MYC2, were upregulated in resistant plants.

WRKY transcription factors regulate defense genes by binding W-box promoter elements (Finatto et al., 2018; Wani et al., 2021). In *Arabidopsis thaliana*, vasculature-expressed *AtWRKY20* activates multiple defensive phytohormones (JA, SA (Salicylic Acid), and ET (Ethylene)) and regulates the spatiotemporal production of plant secondary metabolites during plant-herbivore interactions (Zhao et al., 2019). In rice, *Os*WRKY45 regulates the synthesis of diterpenoid phytoalexins (momilactone, phytocassane, and oryzalexin) by modulating the expression of their biosynthetic genes (Akagi et al., 2014). However, overexpression of OsWRKY89 appears to positively contribute to resistance against *Sogatella furcifera,* by regulating wax content/deposition on the leaf surface (Wang et al., 2007).

The MYC TFs, *MYC2, MYC3,* and *MYC4* genes provide hypersensitivity to the *Spodoptera littoralis* in Arabidopsis. *MYC2*, a key regulator of JA signaling, was detected in resistant induced conditions, consistent with its role in herbivore defense (Fernández-Calvo et al., 2011; Schweizer et al., 2013; Wang et al., 2021). These TFs, either individually or collectively, may activate downstream secondary metabolite pathways via phytohormones, thereby enhancing the expression of these secondary metabolites to counter insect herbivory and promote plant defense response.

4.6. Fatty acids and terpenoid related pathway to plant defense signaling

Herbivory induces a cascade of defense responses in the host plant, which together enhance its resistance to insect attack. PTI and effector-triggered immunity (ETI) exhibit considerable overlap in their signaling mechanisms, often utilizing shared molecular components. A central feature of both defense pathways is their reliance on phytohormone-mediated signaling. Among these, SA and JA are especially prominent for orchestrating plant immune responses (Lim et al., 2017).

In rice, infestation by the brown planthopper (*N. lugens*) induces extensive metabolic reprogramming. Notably, there is upregulation of secondary metabolite biosynthesis, including phenylpropanoid, flavonoid, and terpenoid pathways. Similarly, we observed the upregulation of secondary metabolites related to fatty acids and terpenoids in our study. These alterations lead to increased accumulation of specific defense-related compounds such as schaftoside and isoschaftoside within 24 h of infestation (Uawisetwathana et al., 2019). Complementary metabolomic studies have shown that *N. lugens*-infested rice also exhibits elevated activity in lipid metabolism pathways at different time points, indicating a dynamic and time-resolved defense strategy (Kang et al., 2019).

Jasmonate biosynthesis in plants can proceed through both the octadecanoid and hexadecanoid pathways, contributing to herbivore-induced defense responses. In this study, metabolites related to lipid signaling, including linoleic acid and arachidonic acid, showed increased accumulation following FAW infestation. Linoleic and linolenic acids act as substrates for lipoxygenase (LOX) enzymes and play key roles in jasmonate-mediated defense signaling. Consistently, LOX4 and LOX5 transcripts were upregulated in the resistant genotype, suggesting activation of lipid-derived defense pathways (Turner et al., 2002). Additionally, lipid-mediated immunity involving sphingolipid metabolism has been shown to enhance plant resistance. Overexpression of OsLCB2a1 in *Arabidopsis thaliana* increased sphingolipid intermediates such as sphinganine and phytosphingosine, which strengthened plant defense and reduced aphid infestation (Begum et al., 2016; Chen et al., 2006). Long-chain bases (LCBs) and related genes, including LCB2a, are also associated with the regulation of programmed cell death (PCD), an important mechanism limiting pathogen and insect spread (Saucedo-García et al., 2011).

4.6.1. Terpenoid pathway

Maize utilizes a terpene-based defense system that involves inducible volatile compounds, such as monoterpenes, diterpenes, and sesquiterpenes, which attract natural enemies of herbivores (Aljbory et al., 2018). In addition, non-volatile terpenoid phytoalexins including kauralexins, zealexins, dolabralexins, and β-costic acid contribute to direct defense against insect pests (Block et al., 2019). In our study, FAW-infested resistant maize plants showed increased accumulation of carotenoid-related metabolites, including 5-hydroxyzeaxanthin, meso-zeaxanthin, halocynthiaxanthin, violaxanthin, and siphonaxanthin. Violaxanthin is synthesized from zeaxanthin via zeaxanthin epoxidase (ZEP) through the intermediate antheraxanthin (Takemura et al., 2021).

The diversification of maize terpenoids is largely driven by the expansion and functional variation of terpene synthases (TPSs) and cytochrome P450 enzymes, resulting in a wide range of isoprenoid compounds involved in plant defense (Block et al., 2019). Consistent with this, our transcriptomic analysis revealed induction of *TPS6* and *TPS8* in the resistant genotype following FAW infestation, whereas *TPS1* and *TPS2* were detected in the susceptible genotype. The maize TPS gene family (~30 members) synthesizes diverse terpenoids involved in plant–insect interactions (Chen et al., 2011; Ding et al., 2017). For instance, TPS1 produces monoterpenes such as linalool and geraniol, and sesquiterpenes including (E)-β-farnesene and (E)-nerolidol (Schnee et al., 2002), while TPS2 generates linalool, (E)-nerolidol, and (E, E)-geranyllinalool (Richter et al., 2016). Similarly, TPS6/11 catalyzes the formation of monoterpenes such as β-myrcene and linalool, along with smaller amounts of cyclic monoterpenes including limonene and α-terpinolene, further contributing to maize volatile-mediated defense (Block et al., 2019; Köllner et al., 2008).

4.7. Molecular docking at the predictive target site and its interaction with α-Terpineol

The differential binding affinities of α-terpineol to midgut brush-border enzymes of FAW highlight its potential to selectively disrupt digestive physiology. Among the targets evaluated, Aminopeptidase N (APN) isoforms—particularly APN1—emerged as primary molecular targets. APN1 plays a critical role in terminal protein digestion and also functions as a receptor for insecticidal proteins and phytochemicals (Pigott et al., 2007; Rajagopal et al., 2002). The preferential interaction of α-terpineol with APN1 likely arises from isoform-specific structural features that allow deeper ligand accommodation and greater stabilization through hydrogen bonding and hydrophobic interactions. This selective binding highlights APN1 as a particularly susceptible putative molecular target, warranting further biochemical and functional validation to elucidate its role in α-terpineol–mediated digestive disruption.

In contrast, the moderate binding affinity observed for APN2 and the comparatively weaker interaction with ALP emphasize the influence of structural heterogeneity on ligand specificity. Reduced affinity of APN2 may result from conformational constraints or differences in active-site architecture that limit stabilization of small hydrophobic ligands, consistent with transcriptomic and proteomic evidence of functional divergence among APN isoforms in lepidopteran midguts (Gomes et al., 2025). The predicted binding of α-terpineol near functionally important regions of APN and ALP suggests potential interference with catalytic activity or membrane-associated functions. Previous studies have shown that disruption of these enzymes responsible for digestion, alters membrane permeability, and damages midgut epithelial cells, leading to impaired larval performance. Terpenoids, including α-terpineol, are known to exert antifeedant and cytotoxic effects by modulating enzymes and destabilizing membranes. Together, our docking results provide a molecular framework for α-terpineol-induced digestive stress in FAW, although further validation using biochemical assays, midgut histopathology, and omics-based approaches is required to confirm the physiological relevance of these interactions.

5. Conclusion

This study provides a systems-level perspective on maize responses to fall armyworm through integrated transcriptomic and metabolomic analyses. Resistant genotypes exhibited coordinated transcriptional and metabolic reprogramming involving phytohormone signaling, MAPK cascades, and pathways related to fatty acid and terpenoid metabolism. Several metabolites associated with these pathways, including α-terpineol and carotenoid- and lipid-related compounds, were enriched in resistant lines and were accompanied by differential expression of candidate biosynthetic genes such as *TPS, DXS, LOX, PLD, FAD*, and *ACS*, suggesting their potential roles in maize defense against FAW.

Molecular docking analysis indicated possible interactions between α-terpineol and FAW midgut proteins, providing a preliminary hypothesis for its potential involvement in insect digestive disruption. However, as docking represents a predictive computational approach,

experimental validation through enzyme assays, larval bioassays, and biochemical studies will be necessary to confirm these interactions. Overall, the candidate genes and metabolites identified in this study provide a useful foundation for future functional validation and breeding efforts to improve FAW resistance in maize.

Funding

Funding from CIMMYT International Maize Improvement Consortium for Asia (IMIC-Asia) Project and the OneCGIAR Accelerated Breeding Initiative (ABI) is graciously acknowledged.

CRediT authorship contribution statement

Patne Nagesh: Writing – review & editing, Writing – original draft, Supervision, Resources, Methodology, Conceptualization. **Onkarappa Dhanyakumar:** Writing – review & editing, Writing – original draft, Visualization, Formal analysis. **Jagdish Jaba:** Writing – review & editing, Supervision, Resources. **Kalenahalli Yogendra:** Writing – review & editing, Writing – original draft, Visualization, Validation, Supervision, Resources, Methodology, Formal analysis, Conceptualization. **Jayasaravanan Desika:** Writing – review & editing, Investigation. **Nivedita Shettigar:** Investigation. **Revanayya M. Gothe:** Visualization, Investigation, Formal analysis. **Sagala Murali Mohan:** Investigation. **Pulime Bhaskara Naidu:** Investigation. **Suraj Prashad Mishra:** Investigation. **Sudha K. Nair:** Methodology, Writing – review & editing. **Bindiganavile Sampath Vivek:** Writing – review & editing, Writing – original draft, Visualization, Validation, Supervision, Resources, Project administration, Funding acquisition.

Declaration of competing interest

The authors declare that they have no known competing financial interests or personal relationships that could have appeared to influence the work reported in this paper.

Acknowledgments

The authors acknowledge Rajendra Badbadwal, Venkata Ramana, and Rajendra Prasad for their extensive support and assistance with the laboratory rearing of fall armyworm (FAW). The AI tool ChatGPT (GPT-5 mini) was used only for grammar checking and proofreading. After using this tool, the authors reviewed the content and took full responsibility for the published article. No AI was used to generate scientific content and figures.

Supplementary materials

Supplementary material associated with this article can be found, in the online version, at doi:10.1016/j.stress.2026.101397.

Data availability

The RNA-seq datasets generated in this study have been deposited in NCBI with submission ID SUB15502991 and BioProject ID PRJNA1302109. The metabolomics datasets, and associated metadata, are provided in the Supplementary Tables and are also available in a public metabolomics repository, Metabolites with the accession Id: REQ20260312217753.

References

Akagi, A., Fukushima, S., Okada, K., Jiang, C.-J., Yoshida, R., Nakayama, A., Shimono, M., Sugano, S., Yamane, H., Takatsuji, H., 2014. WRKY45-dependent priming of diterpenoid phytoalexin biosynthesis in rice and the role of cytokinin in triggering the reaction. Plant Mol. Biol. 86, 171–183. https://doi.org/10.1007/s11103-014-0221-x.

Aljbory, Z., Chen, M., 2018. Indirect plant defense against insect herbivores: a review. Insect Sci. 25, 2–23. https://doi.org/10.1111/1744-7917.12436.

Avuthu, T., Sanivarapu, H., Prasad, K., Sharma, N., Sudini, H.K., Yogendra, K., 2024. Comparative metabolomics analysis reveals secondary cell wall thickening as a barrier to resist Aspergillus flavus infection in groundnut. Physiol. Plant 176, e14169. https://doi.org/10.1111/ppl.14169.

Begum, M.A., Shi, X.-X., Tan, Y., Zhou, W.-W., Hannun, Y., Obeid, L., Mao, C., Zhu, Z.-R., 2016. Molecular characterization of rice OsLCB2a1 gene and functional analysis of its role in insect resistance. Front. Plant Sci. 7, 1789. https://doi.org/10.3389/fpls.2016.01789.

Bellota, E., Medina, R.F., Bernal, J.S., 2013. Physical leaf defenses – altered by Zea life-history evolution, domestication, and breeding – mediate oviposition preference of a specialist leafhopper. Entomol. Exp. Appl. 149, 185–195. https://doi.org/10.1111/eea.12122.

Birkenbihl, R.P., Liu, S., Somssich, I.E., 2017. Transcriptional events defining plant immune responses. Curr. Opin. Plant Biol. 38, 1–9. https://doi.org/10.1016/j.pbi.2017.04.004.

Block, A.K., Vaughan, M.M., Schmelz, E.A., Christensen, S.A., 2019. Biosynthesis and function of terpenoid defense compounds in maize (Zea mays). Planta 249, 21–30. https://doi.org/10.1007/s00425-018-2999-2.

Bricchi, I., Bertea, C.M., Occhipinti, A., Paponov, I.A., Maffei, M.E., 2012. Dynamics of membrane potential variation and gene expression induced by Spodoptera littoralis, Myzus persicae, and Pseudomonas syringae in Arabidopsis. PLoS. One 7, e46673. https://doi.org/10.1371/journal.pone.0046673.

Chen, F., Tholl, D., Bohlmann, J., Pichersky, E., 2011. The family of terpene synthases in plants: a mid-size family of genes for specialized metabolism that is highly diversified throughout the kingdom. Plant J. 66, 212–229. https://doi.org/10.1111/j.1365-313X.2011.04520.x.

Chen, M., Han, G., Dietrich, C.R., Dunn, T.M., Cahoon, E.B., 2006. The essential nature of sphingolipids in plants as revealed by the functional identification and characterization of the Arabidopsis LCB1 subunit of serine palmitoyltransferase. Plant Cell 18, 3576–3593. https://doi.org/10.1105/tpc.105.040774.

Chiriboga Morales, X., Tamiru, A., Sobhy, I.S., Bruce, T.J., Midega, C.A., Khan, Z., 2021. Evaluation of African maize cultivars for resistance to fall armyworm spodoptera frugiperda (JE Smith)(Lepidoptera: noctuidae) larvae. Plants 10, 392. https://doi.org/10.3390/plants10020392.

Day, R., Abrahams, P., Bateman, M., Beale, T., Clottey, V., Cock, M., Colmenarez, Y., Corniani, N., Early, R., Godwin, J., 2017. Fall armyworm: impacts and implications for Africa. Outlooks Pest Manag. 28, 196–201. https://doi.org/10.1564/v28_oct_02.

Desika, J., Yogendra, K., Hepziba, S.J., Patne, N., Vivek, B.S., Ravikesavan, R., Nair, S.K., Jaba, J., Razak, T.A., Srinivasan, S., Shettigar, N., 2024. Exploring metabolomics to innovate management approaches for fall armyworm (Spodoptera frugiperda [J.E. Smith]) infestation in Maize (Zea mays L.). Plants 13, 2451. https://doi.org/10.3390/plants13172451.

De Lange, E.S., Balmer, D., Mauch-Mani, B., Turlings, T.C.J., 2014. Insect and pathogen attack and resistance in maize and its wild ancestors, the teosintes. New. Phytol. 204, 329–341. https://doi.org/10.1111/nph.13005.

De Vos, R.C.H., Moco, S., Lommen, A., Keurentjes, J.J.B., Bino, R.J., Hall, R.D., 2007. Untargeted large-scale plant metabolomics using liquid chromatography coupled to mass spectrometry. Nat. Protoc. 2, 778–791. https://doi.org/10.1038/nprot.2007.95.

Davis, F.M., Ng, S.S., Williams, W.P., 1992. Visual rating scales for screening whorl-stage corn for resistance to fall armyworm. Tech. Bull. - Miss. Agric. For. Exp. Stn. 186, 1–9. http://agris.fao.org/agris-search/search.do?recordID=US9406363.

Deshmukh, S.S., Prasanna, B.M., Kalleshwaraswamy, C.M., Jaba, J., Choudhary, B., 2021. Fall Armyworm (*Spodoptera frugiperda*). In: Omkar (Ed.), Polyphagous Pests of Crops. Springer, Singapore. https://doi.org/10.1007/978-981-15-8075-8_8.

Dhanyakumar, O., Naveen, M., Yogendra, K., Jagdish, J., Balasubramani, V., Shanmugam, P.S., Shanthi, M., Murugan, M., 2026. Unlocking nature's arsenal: molecular breeding and biotechnological applications to use plant secondary metabolites against insect herbivores. J. Econ. Entomol. 119 (1), 1–25.

Ding, Y., Huffaker, A., Köllner, T.G., Weckwerth, P., Robert, C.A., Spencer, J.L., Lipka, A. E., Schmelz, E.A., 2017. Selinene volatiles are essential precursors for maize defense promoting fungal pathogen resistance. Plant Physiol. 175, 1455–1468. https://doi.org/10.1104/pp.17.00879.

Erb, M., Meldau, S., Howe, G.A., 2012. Role of phytohormones in insect-specific plant reactions. Trends. Plant Sci. 17, 250–259. https://doi.org/10.1016/j.tplants.2012.01.003.

Erb, M., Reymond, P., 2019. Molecular interactions between plants and insect herbivores. Annu Rev. Plant Biol. 70, 527–557. https://doi.org/10.1146/annurev-arplant-050718-095910.

Fernández-Calvo, P., Chini, A., Fernández-Barbero, G., Chico, J.-M., Gimenez-Ibanez, S., Geerinck, J., Eeckhout, D., Schweizer, F., Godoy, M., Franco-Zorrilla, J.M., 2011. The Arabidopsis bHLH transcription factors MYC3 and MYC4 are targets of JAZ repressors and act additively with MYC2 in the activation of jasmonate responses. Plant Cell 23, 701–715. https://doi.org/10.1105/tpc.110.080788.

Fichman, Y., Mittler, R., 2020. Rapid systemic signaling during abiotic and biotic stresses: is the ROS wave master of all trades? Plant J. 102, 887–896. https://doi.org/10.1111/tpj.14685.

Finatto, T., Viana, V.E., Woyann, L.G., Busanello, C., Maia, L.C.da, Oliveira, A.C.de, 2018. Can WRKY transcription factors help plants to overcome environmental challenges? Genet. Mol. Biol. 41, 533–544. https://doi.org/10.1590/1678-4685-GMB-2017-0232.

Flores-Escobar, B., Rodríguez-Magadan, H., Bravo, A., Soberón, M., Gómez, I., 2013. Differential role of Manduca sexta aminopeptidase-N and alkaline phosphatase in the mode of action of Cry1Aa, Cry1Ab, and Cry1Ac toxins from Bacillus thuringiensis. Appl. Environ. Microb. 79, 4543–4550. https://doi.org/10.1128/AEM.01062-13.

Goergen, G., Kumar, P.L., Sankung, S.B., Togola, A., Tamò, M., 2016. First report of outbreaks of the fall armyworm Spodoptera frugiperda (JE Smith) (Lepidoptera, Noctuidae), a new alien invasive pest in West and Central Africa. PLoS. One 11, e0165632. https://doi.org/10.1371/journal.pone.0165632.

Gomes, A.F.F., Cataldi, T.R., Labate, C.A., Omoto, C., Cônsoli, F.L., 2025. Metabolomics of susceptible and insecticide-resistant strains of Spodoptera frugiperda (Lepidoptera: noctuidae) and metatranscriptomics of their midgut-associated microbiota. Pestic. Biochem. Physiol., 106697 https://doi.org/10.1016/j.pestbp.2025.106697.

Gómez, I., Rodríguez-Chamorro, D.E., Flores-Ramírez, G., Grande, R., Zúñiga, F., Portugal, F.J., Sánchez, J., Pacheco, S., Bravo, A., Soberón, M., 2018. Spodoptera frugiperda (J. E. Smith) aminopeptidase N1 is a functional receptor of the Bacillus thuringiensis Cry1Ca toxin. Appl. Environ. Microb. 84, e01089. https://doi.org/10.1128/AEM.01089-18. -01018.

Gothe, R.M., Karrem, A., Gowda, R.S.R., Onkarappa, D., Jaba, J., Ahn, S.-J., Pathour, S., Yogendra, K., Bheemanahalli, R., 2024. Decoding plant defense: accelerating insect pest resistance with omics and high-throughput phenotyping. Plant Physiol. Rep. 29, 793–807. https://doi.org/10.1007/s40502-024-00835-y.

Harrison, R.D., Thierfelder, C., Baudron, F., Chinwada, P., Midega, C., Schaffner, U., Van Den Berg, J., 2019. Agro-ecological options for fall armyworm (Spodoptera frugiperda JE Smith) management: providing low-cost, smallholder friendly solutions to an invasive pest. J. Environ. Manag. 243, 318–330. https://doi.org/10.1016/j.jenvman.2019.05.011.

Hettenhausen, C., Sun, G., He, Y., Zhuang, H., Sun, T., Qi, J., Wu, J., 2016. Genome-wide identification of calcium-dependent protein kinases in soybean and analyses of their transcriptional responses to insect herbivory and drought stress. Sci. Rep. 6, 18973. https://doi.org/10.1038/srep18973.

Howe, G.A., Jander, G., 2008. Plant immunity to insect herbivores. Annu Rev. Plant Biol. 59, 41–66. https://doi.org/10.1146/annurev.arplant.59.032607.092825.

Hruska, A.J., 2019. Fall armyworm (Spodoptera frugiperda) management by smallholders. CABI Rev. 1–11. https://doi.org/10.1079/PAVSNNR201914043.

Hu, L., Ye, M., Kuai, P., Ye, M., Erb, M., Lou, Y., 2018. OsLRR-RLK1, an early responsive leucine-rich repeat receptor-like kinase, initiates rice defense responses against a chewing herbivore. New. Phytol. 219, 1097–1111. https://doi.org/10.1111/nph.15247.

Kanchiswamy, C.N., Takahashi, H., Quadro, S., Maffei, M.E., Bossi, S., Bertea, C., Zebelo, S.A., Muroi, A., Ishihama, N., Yoshioka, H., 2010. Regulation of Arabidopsis defense responses against Spodoptera littoralis by CPK-mediated calcium signaling. BMC. Plant Biol. 10, 1–10. https://doi.org/10.1186/1471-2229-10-97.

Kang, K., Yue, L., Xia, X., Liu, K., Zhang, W., 2019. Comparative metabolomics analysis of different resistant rice varieties in response to the brown planthopper nilaparvata lugens hemiptera: delphacidae. Metabolomics. 15, 62. https://doi.org/10.1007/s11306-019-1523-4.

Kasoma, C., Shimelis, H., Laing, M.D., 2021. Fall armyworm invasion in Africa: implications for maize production and breeding. J. Crop. Improv. 35, 111–146. https://doi.org/10.1080/15427528.2020.1802800.

Kolanchi, P., Marimuthu, M., Venkatasamy, B., Krish, K.K., Sankarasubramanian, H., Mannu, J., 2025. Phytohormonal signaling network and immune priming pertinence in plants to defend against insect herbivory. Plant Stress 16, 100850. https://doi.org/10.1016/j.stress.2025.100850.

Köllner, T.G., Schnee, C., Li, S., Svatoš, A., Schneider, B., Gershenzon, J., Degenhardt, J., 2008. Protonation of a neutral (S)-β-bisabolene intermediate is involved in (S)-β-macrocarpene formation by the maize sesquiterpene synthases TPS6 and TPS11. J. Biol. Chem. 283, 20779–20788. https://doi.org/10.1074/jbc.M802682200.

Lee, S.-B., Aimanova, K.G., Gill, S.S., 2014. Alkaline phosphatases and aminopeptidases are altered in a Cry11Aa resistant strain of Aedes aegypti. Insect. Biochem. Mol. Bio. 54, 112–121. https://doi.org/10.1016/j.ibmb.2014.09.004.

Lim, G.-H., Singhal, R., Kachroo, A., Kachroo, P., 2017. Fatty acid– and lipid-mediated signaling in plant defense. Annu Rev. Phytopathol. 55, 505–536. https://doi.org/10.1146/annurev-phyto-080516-035406.

Livak, K.J., Schmittgen, T.D., 2001. Analysis of relative gene expression data using real-time quantitative PCR and the $2^{-\Delta\Delta CT}$ method. Methods 25, 402–408. https://doi.org/10.1006/meth.2001.1262.

Malik, G., Chaturvedi, R., Hooda, S., 2021. Role of herbivore-associated molecular patterns (HAMPs) in modulating plant defenses. Plant-Pest Interact.: Mol. Mech. Chem. Ecol. 1–29. https://doi.org/10.1007/978-981-15-2467-7_1.

Matova, P.M., Kamutando, C.N., Magorokosho, C., Kutywayo, D., Gutsa, F., Labuschagne, M., 2020. Fall-armyworm invasion, control practices and resistance breeding in Sub-Saharan Africa. Crop. Sci. 60, 2951–2970. https://doi.org/10.1002/csc2.20317.

Matova, P.M., Kamutando, C.N., Kutywayo, D., Magorokosho, C., Labuschagne, M., 2022. Fall armyworm tolerance of maize parental lines, experimental hybrids, and commercial cultivars in southern Africa. Agronomy 12, 1463. https://doi.org/10.3390/agronomy12061463.

Mithöfer, A., Boland, W., 2012. Plant defense against herbivores: chemical aspects. Annu Rev. Plant Biol. 63, 431–450. https://doi.org/10.1146/annurev-arplant-042110-103854.

Mishra, M., Gupta, K.K., Kumar, S., 2019. Diminished activity of larval midgut transaminases and phosphatases in Helicoverpa armigera Hübner (Lepidoptera) induced by dietary stem extracts of Thevetia neriifolia. J. Lepid. Soc. 73, 23–33. https://doi.org/10.18473/lepi.73i1.a4.

Nagoshi, R.N., Goergen, G., Tounou, K.A., Agboka, K., Koffi, D., Meagher, R.L., 2018. Analysis of strain distribution, migratory potential, and invasion history of fall armyworm populations in northern Sub-Saharan Africa. Sci. Rep. 8, 3710. https://doi.org/10.1038/s41598-018-21954-1.

Nagoshi, R.N., Nagoshi, B.Y., Cañarte, E., Navarrete, B., Solórzano, R., Garcés-Carrera, S., 2019. Genetic characterization of fall armyworm (Spodoptera frugiperda) in Ecuador and comparisons with regional populations identify likely migratory relationships. PLoS. One 14, e0222332. https://doi.org/10.1371/journal.pone.0222332.

Ni, X., Xu, W., Blanco, M.H., Williams, W.P., 2014. Evaluation of fall armyworm resistance in maize germplasm lines using visual leaf injury rating and predator survey. Insect Sci. 21, 541–555. https://doi.org/10.1111/1744-7917.12093.

Onkarappa, D., Pandi, R.K., Gopal, A., Thiruvengadam, V., Muthugounder, M., Nayyar, N., Gopalsamy, S., 2023. Sub-lethal effects of indigenous isolate of Spodoptera frugiperda nucleopolyhedrovirus on fall armyworm growth and reproduction in India. Egypt J. Biol. Pest Control 33, 10. https://doi.org/10.1186/s41938-023-00651-w.

Paiva, L.A.de, Corrêa, F., Silva, C.L.T., Moura, Lima, de, T., Silva, F.C.da, Araújo, Silva, da, M., Jesus, F.G.de, 2016. Resistance of corn genotypes to fall armyworm Spodoptera frugiperda (Lepidoptera: noctuidae). Afr. J. Biotechnol. 15, 1877–1882. https://doi.org/10.5897/AJB2016.15399.

Pigott, C.R., Ellar, D.J., 2007. Role of receptors in Bacillus thuringiensis crystal toxin activity. Microbiol. Mol. Biol. Rev. 71, 255–281. https://doi.org/10.1128/MMBR.00034-06.

Prasanna, B.M., Bruce, A., Beyene, Y., Makumbi, D., Gowda, M., Asim, M., Martinelli, S., Head, G.P., Parimi, S., 2022. Host plant resistance for fall armyworm management in maize: relevance, status and prospects in Africa and Asia. Theor. Appl. Genet. 135, 3897–3916. https://doi.org/10.1007/s00122-022-04073-4.

Prasanna, B.M., Huesing, J.E., Eddy, R., Peschke, V.M., 2018. *Fall Armyworm in Africa: A Guide for Integrated Pest Management*. USAID, 2018, http://hdl.handle.net/10883/19204.

Rajagopal, R., Sivakumar, S., Agrawal, N., Malhotra, P., Bhatnagar, R.K., 2002. Silencing of midgut aminopeptidase N of Spodoptera litura by double-stranded RNA establishes its role as Bacillus thuringiensis toxin receptor. J. Biol. Chem. 277, 46849–46851.

Reddy, A.S., Ali, G.S., Celesnik, H., Day, I.S., 2011. Coping with stresses: roles of calcium- and calcium/calmodulin-regulated gene expression. Plant Cell 23, 2010–2032. https://doi.org/10.1105/tpc.111.084988.

Richter, A., Schaff, C., Zhang, Z., Lipka, A.E., Tian, F., Köllner, T.G., Schnee, C., Preiß, S., Irmisch, S., Jander, G., 2016. Characterization of biosynthetic pathways for the production of the volatile homoterpenes DMNT and TMTT in Zea mays. Plant Cell 28, 2651–2665. https://doi.org/10.1105/tpc.15.00919.

Saucedo-García, M., Guevara-García, A., González-Solís, A., Cruz-García, F., Vázquez-Santana, S., Markham, J.E., Lozano-Rosas, M.G., Dietrich, C.R., Ramos-Vega, M., Cahoon, E.B., Gavilanes-Ruíz, M., 2011. MPK6, sphinganine and the LCB2a gene from serine palmitoyltransferase are required in the signaling pathway that mediates cell death induced by long chain bases in Arabidopsis. New. Phytol. 191, 943–957. https://doi.org/10.1111/j.1469-8137.2011.03727.x.

Schnee, C., Köllner, T.G., Gershenzon, J., Degenhardt, J., 2002. The maize gene terpene synthase 1 encodes a sesquiterpene synthase catalyzing the formation of (E)-β-farnesene,(E)-nerolidol, and (E, E)-farnesol after herbivore damage. Plant Physiol. 130, 2049–2060. https://doi.org/10.1104/pp.008326.

Schweizer, F., Bodenhausen, N., Lassueur, S., Masclaux, F.G., Reymond, P., 2013. Differential contribution of transcription factors to Arabidopsis thaliana defense against Spodoptera littoralis. Front. Plant Sci. 4, 13. https://doi.org/10.3389/fpls.2013.00013.

Sharma, H.C., Singh, F. and Nwanze, K.F., 1997. *Plant resistance to insects in sorghum*. International Crops Research Institute for the Semi-Arid Tropics. PP216.

Soltabayeva, A., Dauletova, N., Serik, S., Sandybek, M., Omondi, J.O., Kurmanbayeva, A., Srivastava, S., 2022. Receptor-like kinases (LRR-RLKs) in response of plants to biotic and abiotic stresses. Plants 11, 2660. https://doi.org/10.3390/plants11192660.

Soujanya, P.L., Sekhar, J.C., Yathish, K.R., Karjagi, C.G., Rao, K.S., Suby, S.B., Jat, S.L., Kumar, B., Kumar, K., Vadessery, J., 2022. Leaf damage based phenotyping technique and its validation against fall armyworm, Spodoptera frugiperda (JE Smith), in maize. Front. Plant Sci. 13, 906207. https://doi.org/10.3389/fpls.2022.906207.

Takemura, M., Sahara, T., Misawa, N., 2021. Violaxanthin: natural function and occurrence, biosynthesis, and heterologous production. Appl. Microbiol. Biotechnol. 105, 6133–6142. https://doi.org/10.1007/s00253-021-11452-2.

Tang, D., Wang, G., Zhou, J.-M., 2017. Receptor kinases in plant-pathogen interactions: more than pattern recognition. Plant Cell 29, 618–637. https://doi.org/10.1105/tpc.16.00891.

Turner, J.G., Ellis, C., Devoto, A., 2002. The jasmonate signal pathway. Plant Cell 14, S153–S164. https://doi.org/10.1105/tpc.000679.

Uawisetwathana, U., Chevallier, O.P., Xu, Y., Kamolsukyeunyong, W., Nookaew, I., Somboon, T., Toojinda, T., Vanavichit, A., Goodacre, R., Elliott, C.T., Karoonuthaisiri, N., 2019. Global metabolite profiles of rice brown planthopper-resistant traits reveal potential secondary metabolites for both constitutive and inducible defenses. Metabolomics. 15, 151. https://doi.org/10.1007/s11306-019-1616-0.

Vashisth, S., Jagdish, J., Sharma, S.P., Sharma, H.C., 2024. Biochemical mechanisms of induced resistance to Chilo partellus in sorghum. Int. J. Pest. Manage 70 (4), 744–755. https://doi.org/10.1080/09670874.2022.2036863.

Wang, D.-D., Li, P., Chen, Q.-Y., Chen, X.-Y., Yan, Z.-W., Wang, M.-Y., Mao, Y.-B., 2021. Differential contributions of MYCs to insect defense reveals flavonoids alleviating

growth inhibition caused by wounding in arabidopsis. Front. Plant Sci. 12. https://doi.org/10.3389/fpls.2021.700555.

Wang, H., Hao, J., Chen, X., Hao, Z., Wang, X., Lou, Y., Peng, Y., Guo, Z., 2007. Overexpression of rice WRKY89 enhances ultraviolet B tolerance and disease resistance in rice plants. Plant Mol. Biol. 65, 799–815. https://doi.org/10.1007/s11103-007-9244-x.

Wang, X., Zhang, Y., Zhang, R., Zhang, J., 2019. The diversity of pattern recognition receptors (PRRs) involved with insect defense against pathogens. Curr. Opin. Insect Sci. 33, 105–110. https://doi.org/10.1016/j.cois.2019.05.004.

Wani, S.H., Anand, S., Singh, B., Bohra, A., Joshi, R., 2021. WRKY transcription factors and plant defense responses: latest discoveries and future prospects. Plant Cell Rep. 40, 1071–1085. https://doi.org/10.1007/s00299-021-02691-8.

War, A.R., Paulraj, M.G., Ahmad, T., Buhroo, A.A., Hussain, B., Ignacimuthu, S., Sharma, H.C., 2012. Mechanisms of plant defense against insect herbivores. Plant Signal. Behav. 7, 1306–1320. https://doi.org/10.4161/psb.21663.

Wu, J., Baldwin, I.T., 2010. New insights into plant responses to the attack from insect herbivores. Annu. Rev. Genet. 44, 1–24. https://doi.org/10.1146/annurev-genet-102209-163500.

Yang, D.-H., Hettenhausen, C., Baldwin, I.T., Wu, J., 2012. Silencing Nicotiana attenuata calcium-dependent protein kinases, CDPK4 and CDPK5, strongly up-regulates wound-and herbivory-induced jasmonic acid accumulations. Plant Physiol. 159, 1591–1607. https://doi.org/10.1104/pp.112.199018.

Ye, M., Kuai, P., Hu, L., Ye, M., Sun, H., Erb, M., Lou, Y., 2020. Suppression of a leucine-rich repeat receptor-like kinase enhances host plant resistance to a specialist herbivore. Plant Cell Environ. 43, 2571–2585. https://doi.org/10.1111/pce.13834.

Zhao, P., Yao, X., Cai, C., Li, R., Du, J., Sun, Y., Wang, M., Zou, Z., Wang, Q., Kliebenstein, D.J., Liu, S.-S., Fang, R.-X., Ye, J., 2019. Viruses mobilize plant immunity to deter nonvector insect herbivores. Sci. Adv. 5, eaav9801. https://doi.org/10.1126/sciadv.aav9801.